Space Weather

RESEARCH ARTICLE
10.1029/2023SW003595

Variability of Ionosphere Over Indian Longitudes to a Variety of Space Weather Events During December 2006

Alok Kuman Ranjan[1], M. V. Sunil Krishna[1], C. Amory-Mazaudier[2], R. Fleury[3], S. Sripathi[4], Geeta Vichare[4], and W. Younas[5]

[1]Department of Physics, Indian Institute of Technology Roorkee, Roorkee, Uttarakhand, India, [2]Laboratoire de Physique des Plasmas (LPP), Sorbonne Université, Ecole Polytechnique, Institute Polytechnique de Paris, Université Paris Saclay, Observatoire de Paris, CNRS, Paris, France, [3]LAB-STICC, UMR, Institute Mines-Telecom Atlantique, Brest, France, [4]Indian Institute of Geomagnetism, Navi Mumbai, India, [5]Laboratory Without Frontiers, International Geophysical Research Group Europe Africa Asia, Paris, France

Abstract This paper highlights the impact of intense solar events over India during 3–20 December 2006. Ionospheric effects of a major solar flare (X9) on December 5 (10:35 UT) have been investigated by using dayside and nightside magnetometer data, dayside ionosondes, and dayside GPS vTEC observations. On the next day, a stream of fast solar wind hits the magnetosphere, causing a HILDCAA (High Intensity Long Duration Continuous Auroral Activity) preceded by moderate geomagnetic storm. The origin and characteristics of a positive ionospheric storm which occurred over Tirunelveli (TIR, geomagnetic latitude: −0.18°N) in the recovery phase of storm due to simultaneous presence of enhanced O/N_2 and WEJ or weakened EEJ during the HILDCAA (7th and 8th of December) is investigated. Subsequently, on December 14, the most powerful CME since the Halloween event impacts the Earth, and three SSCs are recorded on December 14, 16, and 18. The variability of the ionosphere over the Indian longitude sector due to these intense space weather fluctuations is presented by utilizing the magnetometers, ionosonde, GPS vTEC, and satellite-based observations in the same region. This study reports the influence of prompt penetration of the magnetospheric convection electric field and the disturbance dynamo on several key ionospheric and magnetic parameters within the Indian longitude sector.

Plain Language Summary Earth's ionosphere, the ionized portion of the upper atmosphere is highly variable due to atmospheric variations and solar activity. Due to disturbances in the ionospheric electric fields and plasma densities, the ionospheric current systems and their presence on ground-based magnetometers can undergo very complicated changes during space weather events (such as coronal mass ejections (CME), high-speed solar wind (HSS), Co-rotating Interaction Regions (CIRs), solar flares, etc.). In this study, a thorough multi-instrument examination of the ionospheric fluctuations and the accompanying magnetic variations over Indian longitude regions has been done during the several geomagnetic storms between 3 and 20 December 2006 (Solar flare on 5th, CIR induced moderate storm on 6th, following HILDCAA on 7th–8th, and CME induced intense storm on 15th of December in particular). We have also been able to adequately explain the day-to-day fluctuations of the ionosphere over India by taking into account the storm-produced physical events (such as PPEF, DDEF, change in composition, TID, etc.).

Key Points:

- A detailed multi-instrument study of magnetic and ionospheric variation due to a variety of space weather phenomenon in December 2006 over Indian longitudes is presented
- This study shows the signature of the X9 solar flare of 5 December 2006 on the SYM-H and ASY-H indices
- The impact of solar and geomagnetic events on the variation of the Earth's magnetic field due to the ionospheric electric currents is addressed

Supporting Information:

Supporting Information may be found in the online version of this article.

Correspondence to:

M. V. Sunil Krishna,
mv.sunilkrishna@ph.iitr.ac.in

Citation:

Ranjan, A. K., Sunil Krishna, M. V., Amory-Mazaudier, C., Fleury, R., Sripathi, S., Vichare, G., & Younas, W. (2023). Variability of ionosphere over Indian longitudes to a variety of space weather events during December 2006. *Space Weather*, *21*, e2023SW003595. https://doi.org/10.1029/2023SW003595

Received 12 JUN 2023
Accepted 19 OCT 2023

Author Contributions:

Conceptualization: Alok Kuman Ranjan, M. V. Sunil Krishna, C. Amory-Mazaudier, R. Fleury
Data curation: S. Sripathi, Geeta Vichare
Formal analysis: Alok Kuman Ranjan, M. V. Sunil Krishna, C. Amory-Mazaudier, R. Fleury, W. Younas
Investigation: Alok Kuman Ranjan, M. V. Sunil Krishna, C. Amory-Mazaudier, R. Fleury
Methodology: Alok Kuman Ranjan, M. V. Sunil Krishna, C. Amory-Mazaudier, R. Fleury, S. Sripathi

1. Introduction

Thanks to spacecraft like SOHO and Ulysses, among others, a great deal of progress has been made in solar physics during the last two decades. Scientific initiatives such as the International Heliophysics Year (IHY) and the International Space Weather Initiative (ISWI) have improved and guided the research of the influence of solar events on the terrestrial environment. Then, Space Weather was defined to develop a global approach to understand the Sun-Earth system (Lilensten, 2007).

The space weather effects of solar phenomena such as solar flares, Coronal Mass Ejections (CMEs), Co-rotating Interaction Regions (CIRs) are generally felt in Earth's magnetosphere, ionosphere, and atmosphere through the induced perturbation in its ionospheric compositions, electric fields, and wind dynamics. A comprehensive review report on the formation and effects of solar disturbances (CIRs, CMEs, solar flares, Solar Radio Bursts, etc.) linked to space weather was discussed very recently (Gopalswamy, 2022). Enhanced energy and momentum deposition in the form of energetic particle precipitation, Joule heating, and intensified magnetospheric

Project Administration: M. V. Sunil Krishna
Resources: M. V. Sunil Krishna
Software: Alok Kuman Ranjan, M. V. Sunil Krishna, C. Amory-Mazaudier, R. Fleury
Supervision: M. V. Sunil Krishna
Validation: Alok Kuman Ranjan, M. V. Sunil Krishna, C. Amory-Mazaudier, R. Fleury
Visualization: Alok Kuman Ranjan, M. V. Sunil Krishna, C. Amory-Mazaudier, R. Fleury
Writing – original draft: Alok Kuman Ranjan, M. V. Sunil Krishna, C. Amory-Mazaudier, R. Fleury, S. Sripathi, Geeta Vichare, W. Younas
Writing – review & editing: Alok Kuman Ranjan, M. V. Sunil Krishna, C. Amory-Mazaudier, R. Fleury, S. Sripathi, Geeta Vichare

convection in high latitude regions during geomagnetic events result in strong equatorward neutral winds, prompt penetration of electric fields (PPEF) (Vasyliunas, 1970), that can also modify the electrodynamics and compositions of the equatorial to low-latitude ionosphere. Large scale traveling ionospheric disturbances (LSTIDs), and disturbance dynamo electric field (DDEF) can be two of the primary by-products of these disturbances in equatorial to low latitude regions (Blanc & Richmond, 1980; Fujiwara et al., 1996; Mendillo, 2006). A combination of storm-induced compositional changes (O/N_2 ratio), ionospheric electric field perturbations (PPEF and DDEF), thermospheric wind, and TID can affect the distribution of ionospheric plasma density by generating positive and negative ionospheric storms over equatorial to mid-latitude regions (Fuller-Rowell et al., 1994; Prölss, 1993; Ramsingh et al., 2015; Rishbeth, 1998; Rout et al., 2019). Exchange of plasma between the ionosphere and plasmasphere due to ionospheric upflow during geomagnetic storms can result in a decrease in the loss rate of electrons, which can also perturb the ionospheric electron density (Lemaire & Gringauz, 1998).

Multiple X-class solar flares (5, 6, 13, and 14 December) events occurred between the period of 3 and 20 December 2006. Response of the GPS (Global Positioning system) signals to the powerful solar radio bursts (SRBs) associated with these X-class solar flares has been investigated in the past (Afraimovich et al., 2009; Carrano et al., 2009; Cerruti et al., 2008). If flare flux is large enough in *L*-band frequency range with Right-Hand Circular Polarization (RHCP), SRBs associated with the flare might have an impact on GPS performance in terms of reduced carrier to noise (*C*/*N*) ratio of GPS signals in sunlit hemisphere.

An additional atmospheric ionization in the sunlit hemisphere during the solar flare events also causes geomagnetic effects. Solar flare effects (Sfe) are sudden variations in Earth's magnetic field (crochet-like shape), which is mainly attributed to the enhanced conductivity of D-region *or* boundary between D and E-region (below the quiet time dynamo region). However, it was calculated that Sfe is not a simple increase in diurnal variation (Sq). The center of the Sfe current system was found to be a bit higher in latitude (3°–4°N) and 1 hr of local time eastward in comparison to Sq (Curto, 2020; Curto et al., 1994; Gaya-Piqué et al., 2008). In some cases, Sfe can cause magnetic changes in the opposite sense of Sq (reversed Sfe) due to displacement in the ionospheric current system along with the center of its location in both the hemispheres. It was also found that reversed Sfe happens mostly during equinox between 10 and 12 LT with a weaker correlation with solar activity compared to the Sfe.

The progression of December 13 CME in terms of Sun-Earth connection has been studied using MHD-models, in situ, and remote measurements (Kataoka et al., 2009; Liu et al., 2008). The CME was also associated with X3.5 flare with a speed of about 1,775 km/s near the Sun. It produced SRBs, an interplanetary shock (about 1,030 km/s at 1AU), and an intense geomagnetic storm on Earth in subsequent days (Dst-index of about −147 nT) due to magnetic cloud (MC) embedded in the interplanetary CME. The ionospheric and thermospheric response to the initial, and main phase of this geomagnetic storm on 14–15 December has been investigated using both observational and model data sets (Lei et al., 2008; Pedatella et al., 2009). During the initial phase of the storm, a positive ionospheric storm effect occurred in the American longitude sector to the shock associated with the CME. Long lasting positive ionospheric storm in the EIA (Equatorial Ionization anomaly) crest region was also observed over the Pacific Ocean starting from the main phase of the storm for more than 12 hr. It was estimated that the combination of PPEF, equatorward neutral wind, and thermospheric compositions were the source of these positive storms, and the equatorward neutral wind may have played an important role in maintaining it.

In this paper, the thermosphere-ionosphere (T-I) perturbations over the Indian longitude sector due to various space weather events which occurred during 3–20 December 2006 have been investigated. Both ground and space-based observations of key ionospheric and magnetic parameters (magnetometers, ionosonde, GPS-TEC, COSMIC, CHAMP, TIMED/GUVI) have been employed in this study. The data sources and data processing used in this study are presented in Section 2. The solar disturbances and the general geophysical context including the solar wind characteristics and the geomagnetic indices are presented in Section 3. In Section 4, the understanding based on the multi-instrument data of key ionospheric parameters over the Indian longitude region due to solar forcing is presented. The new results obtained by using the recent advances such as wavelet analysis of magnetic field fluctuations due to ionospheric electric fields are presented in Section 5 and subsequently the conclusions are outlined in Section 6.

2. Data Sets and Data Processing

In this study, the response of geomagnetic field, and ionospheric parameters to the continuously occurring multiple space weather events (flares, high intensity long duration continuous auroral activities (HILDCAAs), CMEs

Table 1
Geographic and Geomagnetic Coordinates of the Stations

Station	Geographic latitude (°N)	Geographic longitude (°E)	Geomagnetic latitude (°N)	Geomagnetic longitude (°E)
Magnetometers				
AMS	−37.79	77.6	−46.21	144.9
ABG	18.6	72.9	10.03	146.19
BOU	40.1	−105.2	48.19	−39.29
CLF	48.0	2.3	49.63	85.65
FRD	38.2	−77.4	48.21	−6.62
HER	−34.4	19.2	−33.78	84.07
HON	21.3	−158	21.49	−90.21
SJG	18.11	−66.15	28.04	6.54
TUC	32.3	−110.8	39.83	−43.94
TIR/mag	8.73	77.7	−0.18	149.89
GPS receivers				
HYDE	17.41	78.55	8.34	151.49
IISC	13.02	77.57	4.07	150.15
DGAR	−7.27	72.37	−15.48	142.95
TLSE	43.5	1.5	45.41	83.16
HRAO	−25.89	27.68	−26.99	94.43
JMSM	28.80	83.74	19.24	157.37
IONOSONDES				
Roquetes	40.957	0.333	43.15	81.14
TIR/iono	8.73	77.7	−0.18	149.89

etc.) during 3–20 December 2006 are investigated. The data sets, as well as the techniques used in data processing and analysis for this study, are detailed as follows.

GOES-12 solar X-ray imager (SXI) is used to capture the pictures associated with sudden brightness for all the 4 solar flares (NOAA National Centers for Environmental Information (2022), https://www.ncei.noaa.gov/data/). GOES-13 SXI along with SOHO/EIT (*Extreme ultraviolet Imaging Telescope*, https://www.ias.u-psud.fr/eit/movies/) are used to indicate the dark regions in the solar corona also known as coronal holes. The SOHO satellite images by EIT, and LASCO C2 (C2 camera of the Large Angle and Spectrometric Coronagraph) are also used to capture the strong X3.4 class solar flare along with a coronal mass ejection (CME) that appeared to be headed toward Earth on 13th of December 2006 (https://soho.nascom.nasa.gov/pickoftheweek/old/13dec2006/).

Solar X-ray fluxes measured by GOES 11 are used to observe and identify the occurrence of solar flares with their classes throughout the considered period (NOAA National Centers for Environmental Information (2015), https://www.ngdc.noaa.gov/stp/satellite/goes/dataaccess.html). Table 2 shows the starting, maximum, and end UT time of all the four flares with their classes. The effect of a powerful (X9) solar flare on 5th of December (10:35 UT), in the ionospheric D and E-region is investigated by using 10 magnetometer stations over the globe (Table 1, Figure 1; Black shaded region represents the nightside at 10:30 UT on 5th of December 2006 and black scatter plot represent the magnetic equator). The first 10 stations of Table 1 are also generally used in the estimation of SYM-H, and ASY-H indices. One minute cadence magnetic field data of these stations with their base values for everyday are obtained from International Real-time Magnetic Observatory Network (2006, https://www.intermagnet.org/). The TIR magnetometer data set is obtained on request from Indian Institute of Geomagnetism (IIG, https://www.iigm.res.in/). The base value for TIR magnetometer station is obtained from taking the mean of magnetic field at about midnight during

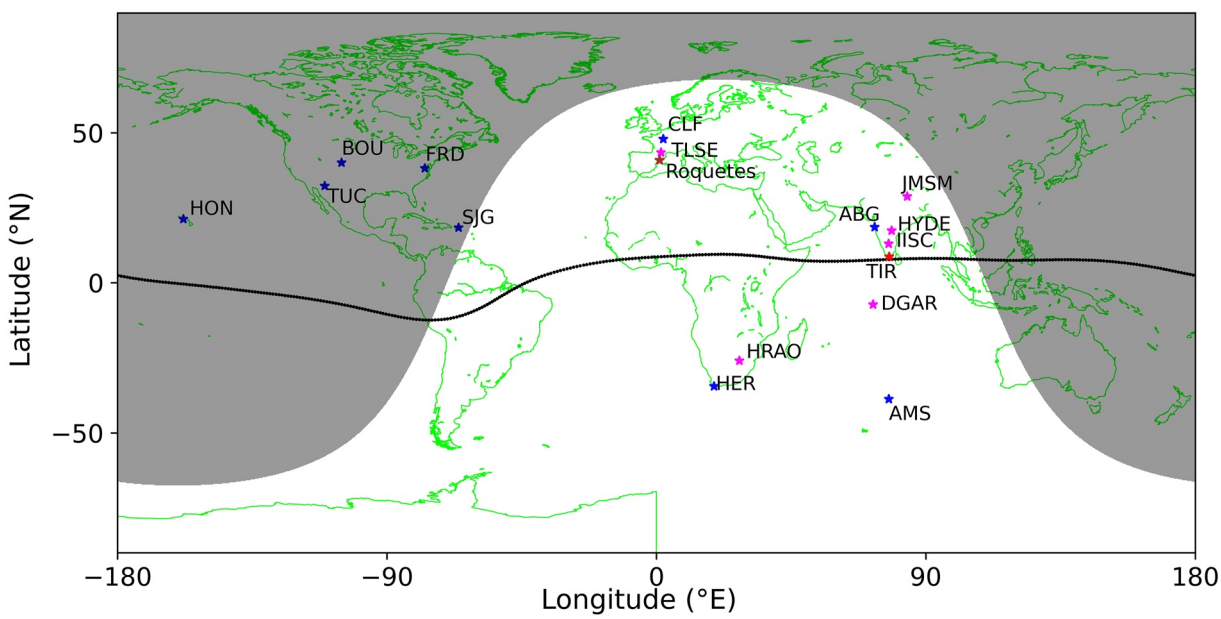

Figure 1. Map with the location of the magnetometers (blue stars), ionosondes (red and brown stars) and GPS receivers (pink stars).

the four International Quiet Days (IQDs; 2, 4, 27, and 29 December) (World Data Center for Geomagnetism, Kyoto (2006), https://wdc.kugi.kyoto-u.ac.jp/qddays/). The base value of each station is subtracted from the measured magnetic field for every day to obtain the variation ΔH (nT).

To characterize the solar, interplanetary, and geomagnetic conditions in this study, solar wind and geomagnetic parameters such as interplanetary magnetic field (IMF) B_0, IMF B_z, solar wind velocity (v), SYM-H, ASY-H, AU, AL, and AE indices are obtained from OMNIWeb interface (Goddard Space Flight Center, OMNIWeb Plus (2006), https://omniweb.gsfc.nasa.gov/). Ap, and Kp indices available at International Service of Geomagnetic Indices (2006, https://isgi.unistra.fr/) are also used to estimate the intensity of the geomagnetic storms.

The O/N_2 ratio calculated using the intensity ratio of oxygen 135.6 nm and N_2 Lyman-Birge-Hopfield emissions from TIMED/GUVI are utilized to show the compositional changes over Indian longitude region throughout the considered period of our study (TIMED/GUVI (2006), https://spdf.gsfc.nasa.gov/pub/data/timed/guvi/). The O/N_2 ratio provided by TIMED/GUVI was referenced to N_2 column density of 10^{17} cm^{-2} to minimize its uncertainties (Strickland et al., 2004; Zhang et al., 2004).

Canadian Advanced Digital Ionosondes (CADI) operating at an equatorial station, Tirunelveli (TIR) (8.73°N, 77.70°E; geomagnetic latitude: −0.18°N) is used to investigate the variations in ionospheric parameters, such as h'F2, and NmF2/foF2 for the considered period.

The daily RINEX files allowing the extraction of vTEC are available on the CDDIS (NASA Earthdata (2006), https://cddis.nasa.gov/archive/gnss/data/daily/) and UNAVCO (NSF's Geodetic Facility for the Advancement of Geoscience (GAGE) (2006), https://www.unavco.org/data/gps-gnss/gps-gnss.html). The Roquetes/Spain ionosonde data sets were consulted on the site (https://ulcar.uml.edu/).

Space-based observations from COSMIC-1 (Constellation Observing System for Meteorology, Ionosphere, and Climate; all six microsatellites, C001 to C006) of electron density profiles and the CHAMP (Challenging Minisatellite Payload) measurement of electron density at about 360 km altitude in the proximity of the TIR ionosonde (7–12°N, 65–80°E), available at University Corporation for Atmospheric Research (2022, https://data.cosmic.ucar.edu/gnss-ro/cosmic1/) and Information System and Data Center, GFZ (2018, https://isdc.gfz-potsdam.de/champ-isdc/access-to-the-champ-data/) (Rother & Michaelis, 2019), respectively, are utilized to complement the TIR ionosonde measured NmF2.

2.1. Processing of Magnetic Field Data

The fluctuations in Earth's equatorial magnetic field (ΔH) in the dayside during geomagnetic storms can be expressed by:

$$\Delta H = S_q + D_{\text{mag}} + D_{\text{iono}} \tag{1}$$

where S_q is the average variance of the Earth's magnetic field on designated magnetic quiet days (ΔH_{quiet}, EEJ emphasis on dayside magnetometers); D_{mag} denotes the magnetic disruption caused by the magnetospheric currents (ring currents, and tail current, etc.) (Fukushima & Kamide, 1973; Le et al., 2004). D_{mag} can be approximated on the dayside at each station by calculating SYM-H cosΦ (magnetic dip latitude Φ is used to standardize the ring current impact at associated station), since it is the largest contributor to dayside magnetospheric currents during extreme space weather conditions.

$$D_{\text{iono}} = \Delta H - S_q - \text{SYM} - H \cdot \cos \Phi \tag{2}$$

D_{iono} is the magnetic disturbance on the dayside due to disturbed ionospheric currents. At low latitudes D_{iono} is related to 2 main physical processes: (a) prompt penetration of the magnetospheric convection electric field PPEF (Vasyliunas, 1970) at the origin of the magnetic disturbance DP_2 (Nishida, 1968), and (b) the ionospheric disturbance dynamo (Blanc & Richmond, 1980), DDEF, at the origin of the magnetic disturbance D_{dyn} (Le Huy & Amory-Mazaudier, 2005).

$$D_{\text{iono}} = \text{DP}_2 + D_{\text{dyn}} \tag{3}$$

To analyze the distinct periods of waves and their existence, a spectrum analysis on D_{iono} is performed with continuous wavelet transform using Morlet wavelet for the duration of our investigation (Nava et al., 2016). To extract the D_{dyn} magnetic disturbance we use the method of wavelet + semblance (Younas et al., 2022).

2.2. vTEC Processing

We used a standard procedure for processing GPS measurements (Hofmann-Wellenhof et al., 1992; Schaer, 1999) and for the conversion of slant TEC to vertical TEC, we use the single layer mapping function (Schaer, 1999), see Azzouzi et al. (2015) for more details. We use the daily measurements of the GPS stations (Table 1) of the International GNSS network (IGS) which are in RINEX 30s format.

The slant Total Electron Content (sTEC) is calculated by combining the two pseudo-range measurements at frequencies $f1$ and $f2$ (Hofmann-Wellenhof et al., 2001). The satellite differential biases (DCB) are obtained from the values published on the website of the University of Bern (ftp.aiub.unibe.ch/CODE/). The receiver bias is estimated by the daily difference between these STEC values on those recalculated from the GIM/CODG model for all the GPS paths and for elevation angles greater than 30° to avoid multi-paths. The use of the single-layer ionospheric model mapping makes it possible to calculate the vTEC (v for Vertical) from the calibrated sTEC considering the altitude of the IPP point (Ionospheric Positioning Point) at 420 km.

3. Global Sun-Earth Contexts

To specify the Sun-Earth context we characterize the Solar disturbances (solar flare, coronal hole, and CME) in Section 3.1 and the solar wind variations and geomagnetic indices in Section 3.2.

3.1. The Solar Events: Solar Flare, Coronal Hole, and CME

All the four X-class solar flares that occurred during our period of investigation (5, 6, 13, and 14 December 2006, respectively) are shown in the first row of Figure 2 with a sudden variation in brightening captured by GOES-12 SXI. The origin of all these flares was active sunspot region 10,930. The abrupt increase in electromagnetic emissions during a flare at different wavelengths (from radio waves to gamma rays) can be responsible for the rapid ionospheric disruptions and subsequent perturbation of the Earth's magnetic field known as magnetic crochet. Solar flares are facets of energy released from closed field lines on the Sun, while coronal holes comprise open field lines to space where solar plasma can radially escape as high-speed streams (HSS). Soft X-rays, and EUV pictures by GOES-13 SXI, and SOHO/EIT (second row of Figure 2) show solar coronal holes as dark patches, because of their colder and less dense plasma characteristics than surroundings. As the fast HSS associated with a coronal hole interact with background solar wind a co-rotating interaction region (CIR) forms with fluctuating IMF-B_z polarity, which can result in low to moderate space weather activity after the interaction with Earth's magnetosphere (Tsurutani et al., 2006).

CMEs are the most dramatic eruptions in the solar corona that have been identified as main contributors of interplanetary disruptions. SOHO/LASCO C2, and SOHO/EIT both observed a strong halo CME accompanied by X3.4 flare on December 13 (bottom row of Figure 2, as it was also observed by GOES-12, first row, 3rd figure from the left). It was the largest halo CME since the Halloween storms (Liu et al., 2008). After interacting with Earth's magnetosphere, this CME produced an intense geomagnetic storm on 14th–15th of December. This paper goes into further detail on the impact of solar flares, coronal holes, and the CME on the Earth's ionosphere and magnetosphere.

Figure 3 depicts the solar X-ray fluxes (Watts.m^{-2}) observed by the GOES-11 Solar X-ray Imager during 3–20 December that included four X-class flares. The blue, and red curves in the figure denote the short wavelength (0.05–0.3 nm), and long wavelength (0.1–0.8 nm) X-ray irradiances, respectively. The vertically green dotted lines represent the maximum of these X-class flares, in which the X9 flare on December 5 is the most powerful of the four in terms of X-ray output. The effects of the SRBs associated with these flares on the ionosphere, and GPS functioning has been studied in the past (Afraimovich et al., 2009; Carrano et al., 2009; Cerruti et al., 2008). The starting, maximum, and the end time of these flares are also provided in Table 2. The sudden brightening at the Sun about the maximum of these flares was also captured by the GOES-12 SXI, which is also shown in the first row of Figure 2 (from left to right, X9: 5 December (10:37 UT), X6.5: 6 December (18:45 UT), X3.4: 13 December (2:40 UT), X1.5: 14 December (22:15 UT)).

3.2. Solar Wind and Geomagnetic Parameters From 3 to 20 December

Figure 4 illustrates the characteristics of the solar wind and the geomagnetic parameters. Panels from the top to bottom are plotted as (a) the solar wind magnetic field B_0 and the B_z component in nT, (b) the speed of the solar

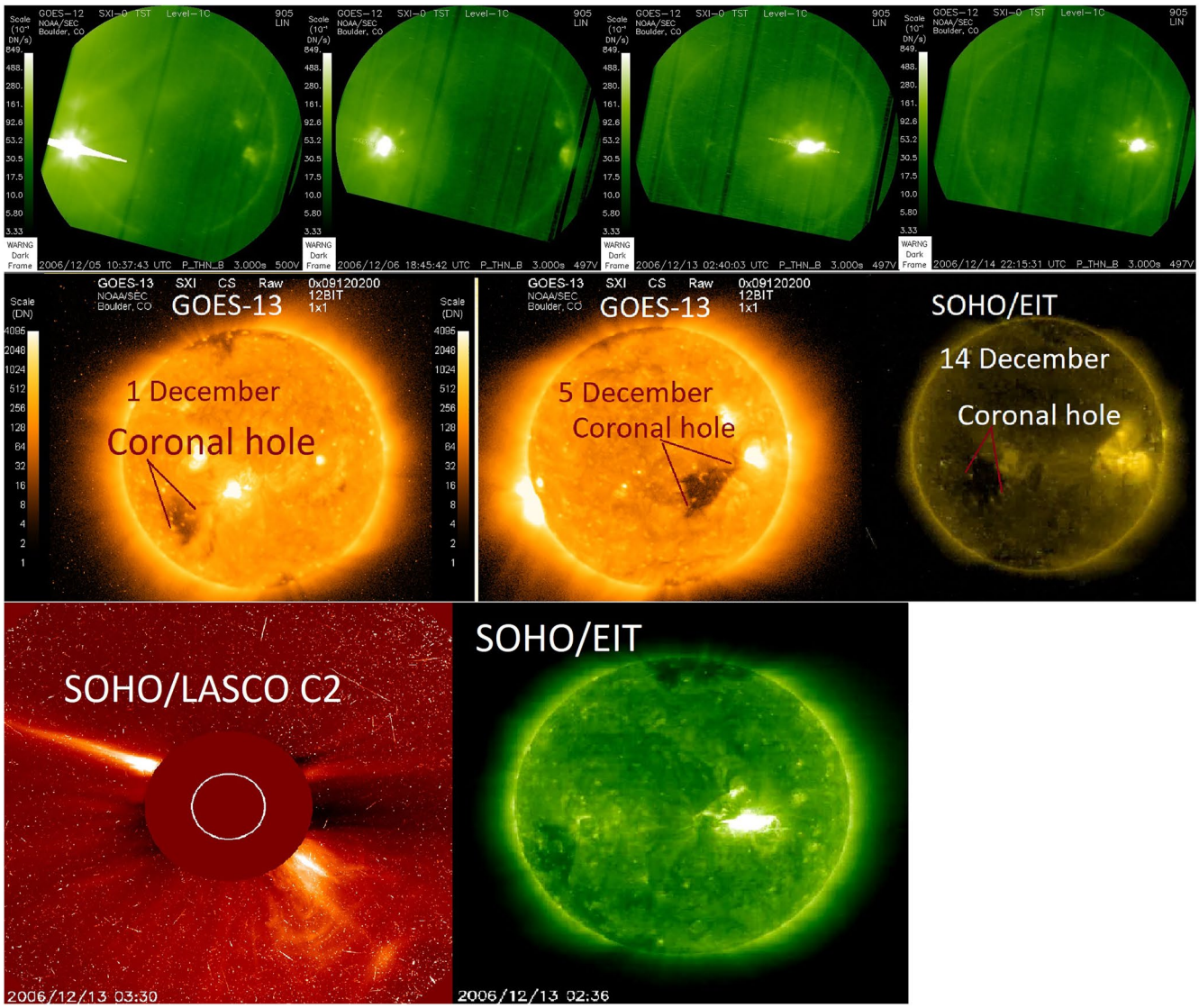

Figure 2. First order observation of selected Solar events for this study: Solar Flares (https://www.ncei.noaa.gov/data/), Coronal holes (https://www.ias.u-psud.fr/eit/movies/), and CME by SOHO and GOES instruments (https://soho.nascom.nasa.gov/pickoftheweek/old/13dec2006/) (see the text for more details).

wind in km/s, (c) the Ap index, (d) the Kp index, (e) the SYM-H and ASY-H indices and (f) AE, AU, and AL magnetic indices.

The solar wind profile along with the occurrence of strongest X9 solar flare of 5 December, and the geomagnetic indices during the period of 3–20 December are shown in Figure 4. As discussed earlier, the X9 flare (shown as a vertical green dotted line) was associated with the active region 10,930 and lasted for about 28 min (Table 2). It can be seen in Figure 4 that the geomagnetic conditions on the Earth are very quiet before this flare, which could be due to the particular location of the flare (solar eastern limb, Figure 2). However, the effects of solar energetic particles (SEPs) associated with this flare were observed at Venus, and Mars (Futaana et al., 2008). The effect of this flare on Earth's magnetic field around the globe is discussed in the next section. Enhanced geomagnetic activity, as observed in geomagnetic indices (Figures 4c–4f) just after the sudden storm commencement (SSC) at 23:59 UT on 5th of December could be due to the coronal holes shown in Figure 2 (5 December). The CIR associated with southward IMF-B_z (Figure 4a) caused by the coronal hole could have played an important role in creating a low to moderate geomagnetic activity on 6th of December. This geomagnetic activity was then followed by High Intensity Long Duration Continuous Auroral Activities (HILDCAAs) on 7th and 8th of December due to continuous fluctuation in the polarity of IMF-B_z associated with the CIR. Before the geomagnetic conditions

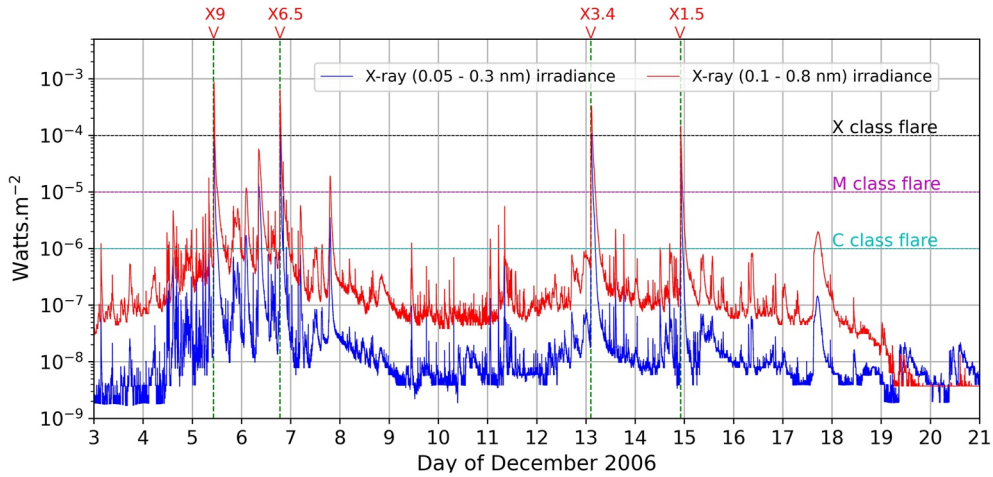

Figure 3. GOES-11 observational data on the solar flares from 3 to 20 December 2006.

could come back to their quiet time values, increasing solar wind speed, and fluctuating polarity of IMF-B_z again resulted in low-to-moderate geomagnetic activities from late UT hours of 9th December to 12th December.

An earthward directed coronal mass ejection accompanied by X3.4-class flare (Figure 2, bottom row) occurred in the early UT hours of 13 December. A sharp increase in solar wind speed (Figure 4b) from about 590 to 980 km/s with an SSC (Sudden Storm Commencement) at about 14:14 UT on 14th of December was detected as a CME shock. After this shock, the solar wind speed began to fall along with the shifting IMF-B_z polarity, resulting in increased geomagnetic activity. The sudden northward to southward turning of IMF-B_z at about 23:05 UT on the same day started the main phase of an intense geomagnetic storm. As a result, the SYM-H index reached a minimum of about −200 nT in the early UT hours of 15 December, after which the recovery phase of the storm began. A detailed investigation of this particular CME utilizing combined remote sensing, in situ, modeling data sets is provided in Liu et al. (2008). A low to mid geomagnetic activity as indicated by geomagnetic indices during 19–20 December could be linked with the CIR associated with the coronal hole of 14 December shown in Figure 2. The UT hour occurrence of all the five SSC during the period of investigation is also presented in Table 3.

4. Results

This section is organized taking into account the different solar disturbances and their effects on Earth's ionosphere. In Section 4.1 we analyze the impact of the X9 Solar flare on the Earth's magnetic field, the F2 region of the ionosphere and the vTEC. In Section 4.2, we analyze the impact of CIR and CME on the ionosphere, for this we study the F2 region of the ionosphere, the vTEC and the O/N_2 ratio. In Section 4.3 we also investigate the impact of CIR and CME on the Earth's magnetic field and we use signal processing techniques to separate the signatures of different physical processes (PPEF and DDEF).

Table 2
Table of X Solar Flares

Date (dd/mm/YYYY)	Flare class	Start time (UT)	Maximum (UT)	End time (UT)
05/12/2006	X9	10:18	10:35	10:45
06/12/2006	X6.5	18:29	18:47	19:00
13/12/2006	X3.4	2:14	2:40	2:57
14/12/2006	X1.5	21.07	22:15	22:26

4.1. Impacts of X9-Flare of December 5 on the Earth's Magnetic Field and vTEC

4.1.1. Impact of the X9-Flare on the Earth's Magnetic Field

Figure 5 shows the magnetic field variations on December 5 observed in 10 magnetic stations (Table 1, Figure 1) located on the dayside and nightside, at the bottom of the figure the magnetic indices SYM-H and ASY-H are also plotted. Based on the local time of each considered magnetometer station (Figures 5a–5j) at the time of the flare (10:35 UT, represented in green), the stations in the sunlit hemisphere (AMS, CLF, HER, SJG, TIR, ABG) detected solar flare effects (Sfe) as a rapid drop or rise (crochet-like shape) in the horizontal component of the Earth's magnetic field compare to the

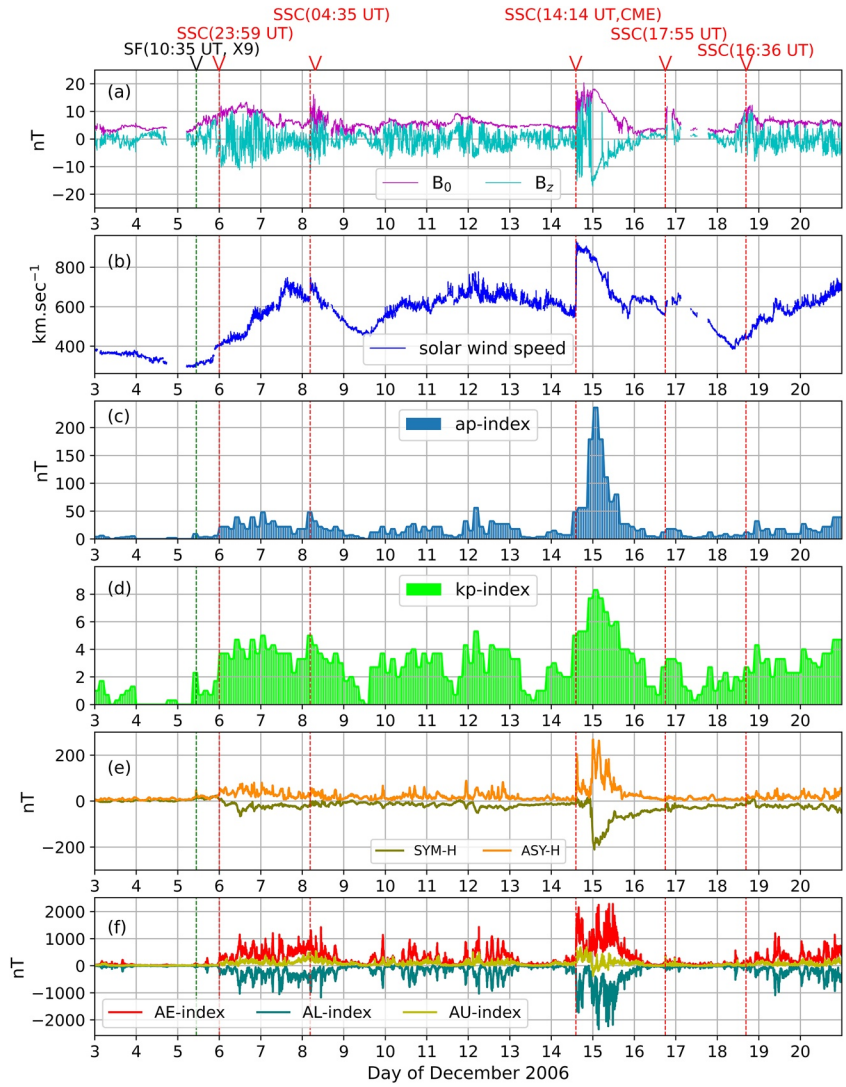

Figure 4. Solar wind and magnetic parameters from 3 to 20 December 2006, (a) solar wind magnetic field B_0 and B_z in nT, (b) solar wind speed in km/s, (c) magnetic index Ap in nT, (d) Kp index, (e) SYM-H and ASY-H in nT, (f) AE, AU and AL indices in nT.

quiet time variations. The stations chosen in Figures 5a–5j are the stations over the globe (except for TIR), which are generally used in the estimation of SYM-H/ASY-H indices. It can be seen in Figures 5k and 5l that the presence of this sudden disturbance in the magnetic field is also present in ASY-H, and SYM-H indices as a sudden increase. The effect on another M1.8-class at about 8 UT (lime vertical dotted line) on the same day can also be seen at TIR station as a sudden enhancement in earth's magnetic field. The effects of other three solar flares mentioned in Table 2 are also present in the dayside magnetometer stations minutes after the UT occurrence of the flares (figure not shown). The stations which show the largest perturbations are different than presented in Table 1, that's why their effects are not found in SYM-H/ASY-H indices as strong as X9 flare.

Table 3
Table of SSCs (Sudden Storm Commencements)

Year	Month	Day	hhmm
2006	12	05	2359
2006	12	08	0435
2006	12	14	1414
2006	12	16	1755
2006	12	18	1636

During the solar flare events, the enhanced conductivity of D-region *or* boundary between D and E-region (below the quiet time dynamo region) due to additional atmospheric ionization in sunlit hemisphere plays an important role in Sfe variations presented above (Curto, 2020; Curto et al., 1994; Gaya-Piqué et al., 2008; Rastogi et al., 1999; Sripathi et al., 2013). It was

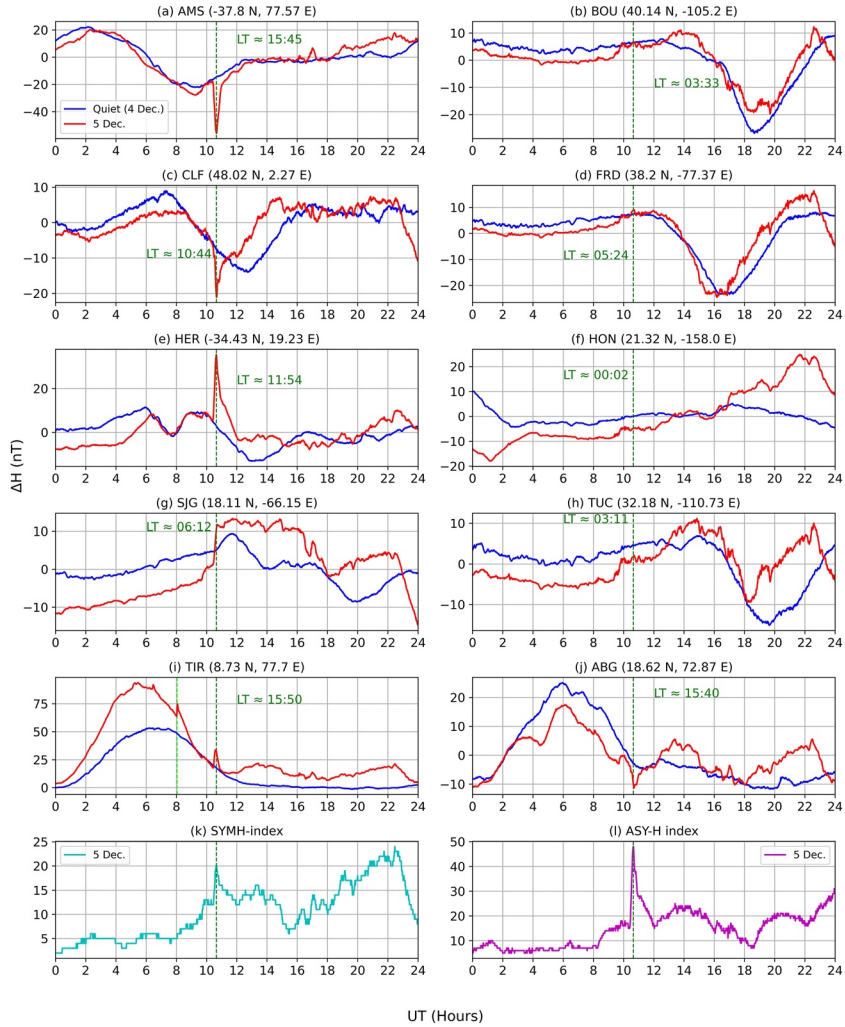

Figure 5. Impacts of the solar flare on the Earth's magnetic field on 5 December 2006.

calculated that the Sfe are not just intensified diurnal variation (Sq) as the location of the Sfe current system can be a bit higher in latitude (3°–4°N) and 1 hr of local time eastward in comparison to Sq. The relocation of the ionospheric current system and its center may sometimes generate magnetic changes in the opposite sense of Sq (reversed Sfe) in both hemispheres. The ionospheric effects of this flare are discussed further ahead.

4.1.2. Impact of the X9-Flare on vTEC

The total electron content (TEC) is an essential property of the total ionization level in Earth's atmosphere. In the GPS era, global measurements of vertical TEC (vTEC) can assist us in estimating the effects of space weather disturbances on the ionosphere (Tsurutani et al., 2009). Figure 6a illustrates the vTEC measurements by the GPS satellites with different PRN (Pseudo random noise) number at different GPS receivers (TLSE-prn06, HRAO-prn09, for middle latitudes; IISC-prn24, DGAR-prn02, for low latitudes with positions provided in Table 1) on 5th of December during the occurrence of X9 flare. The three blue vertical lines at each receiver represent the beginning, maximum, and end UT hour, respectively, of the X9 flare (Table 2). As all the receivers shown in the figure are in the dayside at the time of the flare, it can be seen that after about 7–9 min from the beginning of the flare, TEC starts an abrupt increase at each station, and reaches a total increment of 1.2–1.4 tecu (1 tecu = 10^{16} el/m^2) for middle latitudes and less than 1.0 tecu at low latitudes. These values are significantly lower than the increases of 25 tecu preserved during the Halloween events of 2003 (Tsurutani et al., 2005). This increase in TEC at each station is due to the enhanced/additional ionization caused by the extreme ultraviolet and X-rays bands that radiated during the solar flare. This enhanced ionization of iono-

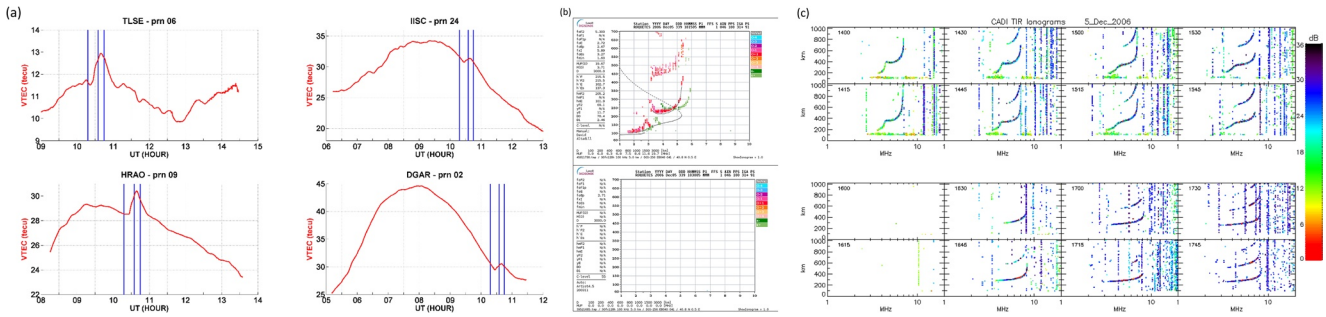

Figure 6. (a) Impact of the solar flare on GPS receivers TLSE, IISC, HRAO, and DGAR. (b) Impact of the solar flare on the ionosonde of Roquetes/Spain. (c) Impact of the solar flare on the ionosonde at TIR/India.

spheric D and E-layers during large flares is important but the region is limited in altitudes so the increase of TEC is of few TEC units. Normally, the maximum is near the sub-solar point but in our case, the increase is maximum in middle latitudes. The increase in TEC lasts about 50 min and therefore is maintained well beyond the end of the solar flare.

In the D layer, the frequency of collisions with the neutral particles is also important, an increase in the number of electrons strongly increases the absorption of the radio waves which cross it and in particular the HF waves (3–30 MHz). For the sounding of the ionosphere by ionosondes, the consequence is an absence of echoes from the first HF frequencies which can lead to a total blackout on all frequencies for several tens of minutes during strong flare eruptions (Chakraborty et al., 2018; Tao et al., 2020). Figures 6b and 6c illustrate this phenomenon. On both the stations of Roquetes (Spain) and TIR (India), echoes from regions E and F are present at 10:15 UT. At 10:30 UT (16:00 IST), there is a total radio fadeout with even the disappearance of jammers.

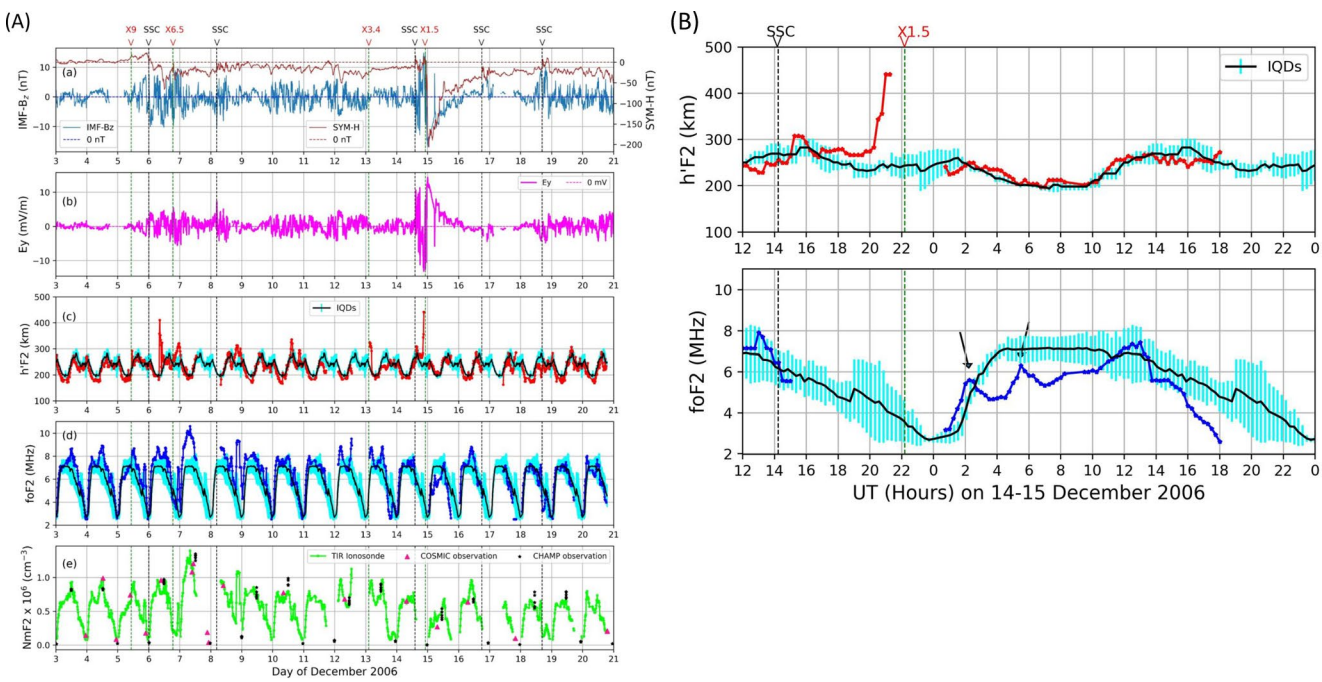

Figure 7. (A) From 3 to 20 December 2006, (a) solar wind data IMF B_z, and SYM-*H* index, (b) Interplanetary electric field Ey in mV/m, (c) h′F2 at TIR, (d) foF2 at TIR, (e) NmF2 at TIR compared with CHAMP and COSMIC-1 observational data. (B) Zoom on ionosonde data at TIR on 14–15 December 2006.

4.2. Impacts of CIR and CME on Ionosphere

4.2.1. Impact of CIR and CME on the F2 Ionospheric Layer

Figure 7A is composed of 5 panels, the first panel shows the UT variations in solar wind parameter (IMF-B_z), and geomagnetic index (SYM-H index) from 3 to 20 December. The second panel shows the variation in the eastward (*or* dawn to dusk) component of the interplanetary electric field (IEF-E_y) imposed on earth by the solar wind. The next two panels show the temporal variations of h′F2, and foF2, respectively, with background quiet days as observed by the TIR ionosonde for the same period. The bottom panel illustrates the variations of NmF2. The green and black vertical lines represent the occurrence of solar flares, and sudden storm commencements (SSCs), the strength of each flare is also mentioned at the top of the figure.

In general, the foF2 are above the median at the beginning of the month (from 03 to 13) and below at the end of the period. We see two diurnal maximums on foF2 (e.g., days 04, 06, 08, 12, 13, 16, 20), one in the morning and the other in the afternoon with a decrease around local noon ("bide-out") (Chen et al., 2021; Kane, 2006). This is typical of low latitudes.

On the top panel, the variations of the B_z component of the solar wind magnetic field represents the signature of the different solar events. The oscillatory variations reveal the presence of CIR. A first CIR arrived on December 6 and peaked at a speed ∼700 km/s on December 7 (see Figure 4 panel b), a second CIR arrived on December 10 which peaked on December 12 at a speed of ∼700 km/s (see Figure 4 panel b). Then on December 14 and 15, the impact of a CME and negative B_z component of the solar wind magnetic field was observed (see Figure 4 panel a). At the end of December 18, a new third CIR was also observed. The two CIRs produced an increase in the foF2 component at TIR, on December 7 and 8 for the first CIR, and on December 12 and 13 for the second CIR. The increase of foF2 was observed to be 2 MHz on December 7 and about 1 MHz on December 8, 12 and 13. The foF2 reached up to about 10.5 MHz over Tirunelveli (Mag. Lat. = −0.18°N) near local noon on 7th. The impact of the CME was very different. On December 15th, a decrease of foF2 by 2 MHz as well as the presence of an oscillation of the foF2 were observed, and on December 16th a small increase in foF2 was also observed.

The first CIR produced a positive ionospheric storm and the CME a negative storm followed by a positive ionospheric storm. The CME caused an intense magnetic storm with strong negative SYM-H values. Geomagnetic storms generally produce a negative ionospheric storm in summer hemisphere and positive ionospheric storm in winter hemisphere (Fuller-Rowell et al., 1996) except for strong geomagnetic storms where there is a negative phase in the winter hemisphere too. This scenario seems to fit the observations. Concerning the decrease of foF2 (negative ionospheric storm) observed on December 15th, it is also well explained by UT time of the beginning of the storm (Fuller-Rowell et al., 1994).

The last panel of Figure 7A represents the variation in NmF2 (*computed from foF2*) measured by TIR ionosonde (lime color). The magenta triangle and black asterisk scatter points indicates the NmF2 measured by COSMIC-1 and electron density measured by CHAMP (at about 360 km), respectively, in the vicinity of TIR ionosonde (7–12°N, and 65–80°E) for the same time period. It can be seen in the Figure that the COSMIC-1 and CHAMP observations agree with the TIR ionosonde to a large extent throughout the considered period of the study. For example, the positive ionospheric storm on 7th of December is evident in all three instruments, along with the negative ionospheric storm observed on 15th of December.

Another interesting feature of the figure is the presence of Traveling Ionospheric Disturbances (TIDs) in the foF2 just after the main phase of an intense geomagnetic storm on 15th of December. A zoom part of Figure 7A on 15th of December is also shown in Figure 7B. Figure 7B depicts the TIDs present in the early UT hours indicated by the arrows. The presence of both the peaks are at about 2.25 UT, and 5.5 UT, respectively, which is just before the UT time when the same TIDs are observed near IISC in measured vTEC (Figure 8b). There are also sudden enhancements in h'F2 during the earlier mentioned main phase of moderate storm on 6th of December, and the main phase of intense storm near the midnight of 14th of December.

4.2.2. Impact of CIR and CME on vTEC

To comment on the temporal variations of vTEC during this period, we use the daily solar flux over 10.7 cm measured in Ottawa as a proxy (figure not shown) for ionizing solar radiation. It presents a maximum of 100 sfu around 05–06/12 and decreases steadily toward a minimum of 70 sfu (−30%) on 20/12. For the 3 stations (JMSM, IISC, and HYDE) the maximum of vTEC diurnal trend is observed around 08–09/12 and it decreases to reach a minimum on 29/12 (figure for *x*-axis limit 21–31 December not shown, Figure S1). The date of the

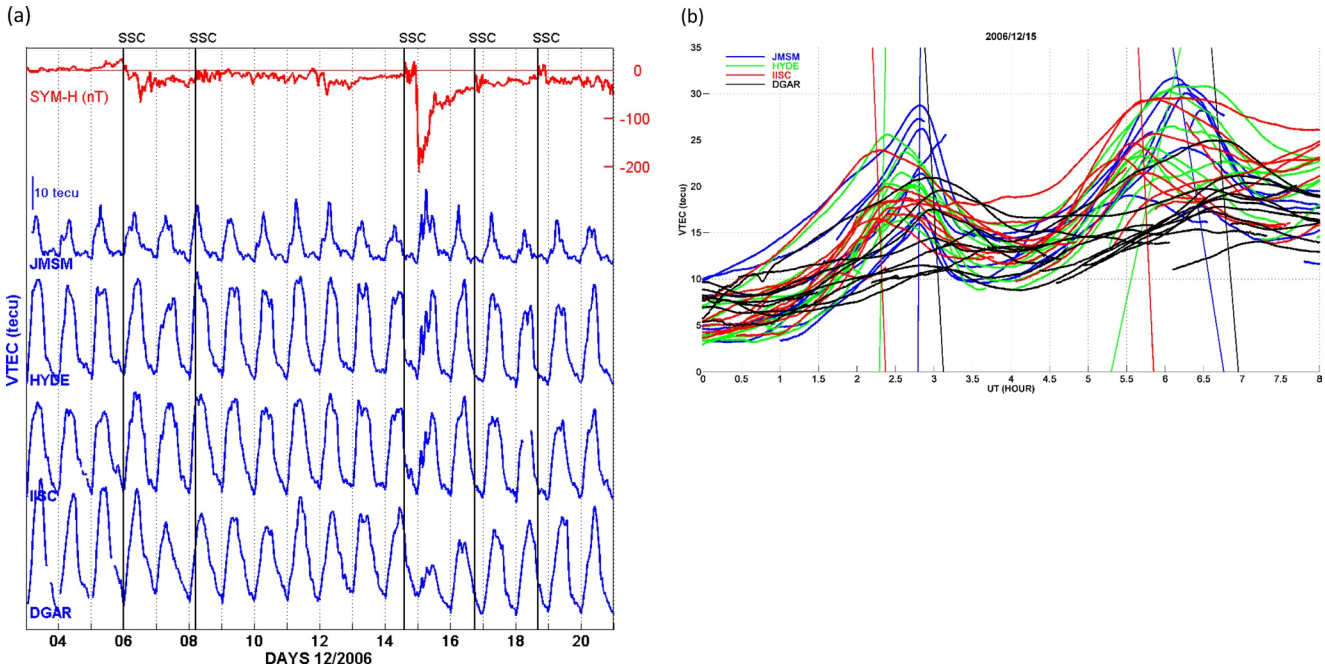

Figure 8. (a): On the top sub-figure the variations of SYM-H, and vTEC measured in various GPS stations in Asia: JMSM, HYDE, IISC, and DGAR from December 3 to 20. (b) Zoom on the vTEC observations on December 15.

maximum occurs a few days after that of the solar flux indicating a reaction time of the ionosphere. We find in the daily evolution of the vTEC that of the 27-day rotation of the Sun. On the other hand, for the DGAR station in the southern hemisphere, the evolution is different with a maximum on 03–04/12, a minimum level on 15/12 and a second diurnal maximum on 26/12. The level of ionization at this station strongly depends on the presence of a southern equatorial crest and its geographical position.

Figure 8a is divided into five panels; the first (from the top) panel shows the temporal variation of SYM-H index (nT) throughout 3–20 December 2006 (red color). The last four panels show the temporal variation in vTEC (tecu) at JMSM, HYDE, IISC, and DGAR GNSS stations, respectively (Table 1). The vTEC levels increase as the day begins, peaking before sunset and then decreasing as the day concludes. The five vertical black lines represent the UT occurrence of SSCs for the same period (Table 3). It is noticeable in the figure that there is a significant decrease in vTEC at DGAR (Table 1; Mag. Lat. = −15.48 N, near southern equatorial ionization anomaly (EIA) crest) at about local noon on 7th of December. As it will be discussed later that, there is a westward electrojet (WEJ) present at the same time (near local noon) in the Indian longitude region, which can cease the fountain effect, and hence the less vTEC observed at the same time compared to previous quiet day (4th of December). The JMSM station (Mag. Lat. = 19.24 N) is also near the northern EIA crest region, however, there is no depletion in vTEC there. The enhanced O/N_2 ratio near the JMSM station (Figure 9e) may compensate for the effect of WEJ, which results in negligible perturbation of vTEC compared to quiet days at JMSM near local noon on 7th of December. Another evident change in vTEC occurred on 15th of December, when DGAR station showed a depleted vTEC, which could be due to large depletion of O/N_2 ratio at the same location (Figure 9m). An interesting feature of Figure 8a is the presence of traveling ionospheric disturbances (TIDs) in the vTEC measured at all the mentioned GNSS stations on 15th of December. Figure 8b shows the zoom on vTEC profiles at each of the four stations (color coded) on 15th of December from 0 to 8 UT. The zoom on the two maximum of 15 December on the fof2 (Figure 7B) goes in the same direction as the vTEC (Figure 8b) and we do not see any notable movement on h′F (evolution in slight descent). We can hypothesize that these undulations are only at the level of the F2 region and do not concern the upper ionosphere or little above 400 km.

4.2.3. Impact of CIR and CME on the Ratio O/N_2

The thermospheric-ionospheric response to the geomagnetic storm time joule heating and accompanying thermospheric dynamics changes is also controlled by the local time at the start of the storm and the season (Fuller-Rowell

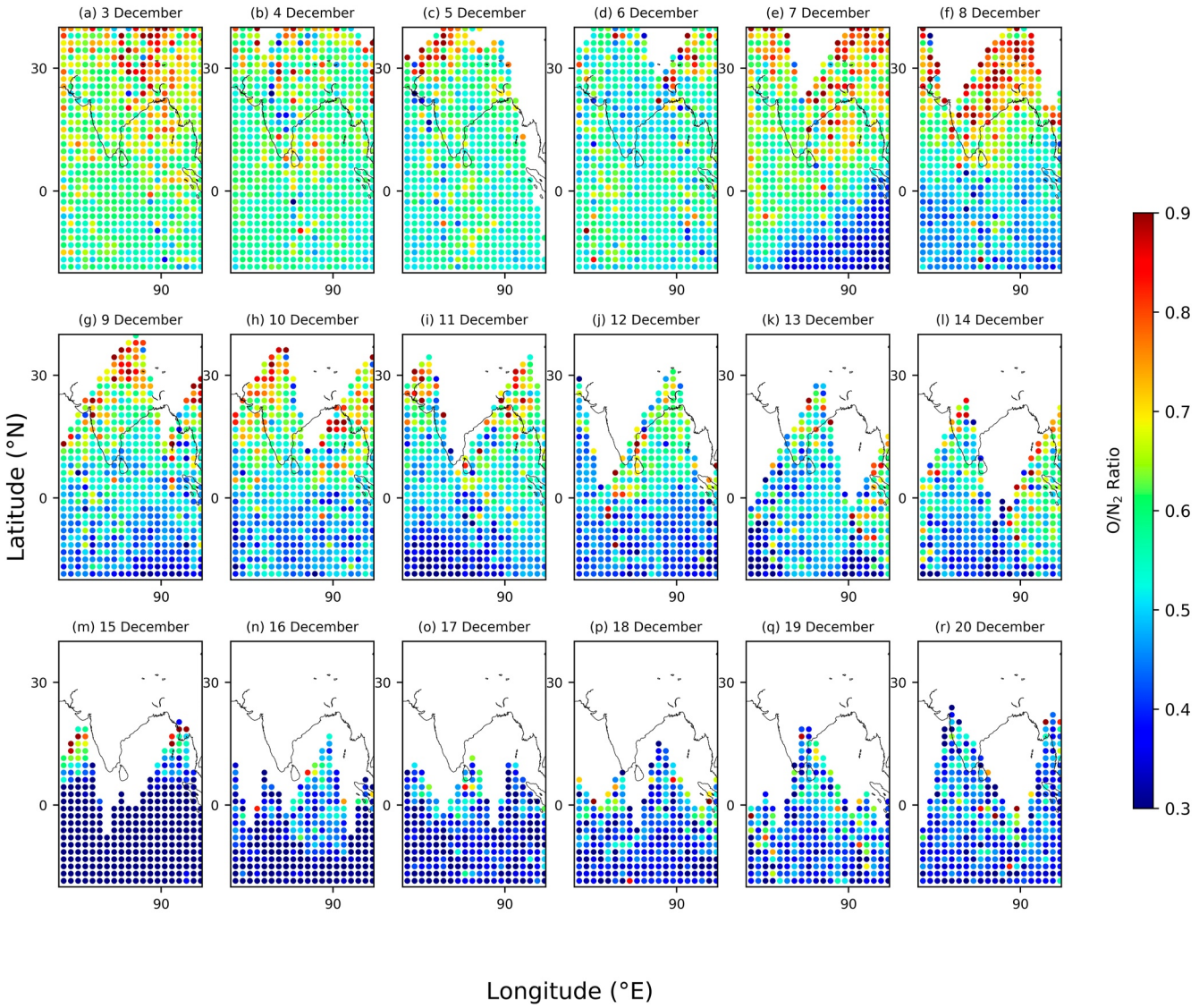

Figure 9. TIMED/GUVI observed O/N_2 data over India from 3 to 20 December 2006.

et al., 1994, 1996). The compositional changes (mostly in O/N_2 column density) in the thermosphere caused by storm-induced dynamics play a major role in determining the positive/negative phases of ionospheric storms.

Figures 9a–9r shows the TIMED/GUVI observed O/N_2 variations in Indian latitude-longitude regions from about 9:30 to 12:30 LT throughout 3 to 20 December 2006. It can be seen in the Figure that after the first CIR induced moderate storm on December 6th, a continuous auroral activity (HILDCAA) after the main phase of the storm (Figures 4e and 4f) resulted in O/N_2 enhancement in equatorial-low latitude regions of winter (northern) hemisphere with depletion in mid-low latitude summer (southern) hemisphere on 7th and 8th December (Figures 9e and 9f). The TIMED/GUVI data set isn't available for the whole globe at the time, however it is evident in Figure 9m that, there was a depletion in O/N_2 ratio again in equatorial region which even penetrated toward the winter hemisphere just after the CME induced intense geomagnetic storm on December 15th. After that, the O/N_2 ratio starts coming back to its pre-storm values (Figures 9p–9r).

4.3. Impacts of CIR and CME on the Earth's Magnetic Field

During magnetic storms, two large scale disturbances processes of ionospheric electric currents act at low latitudes.

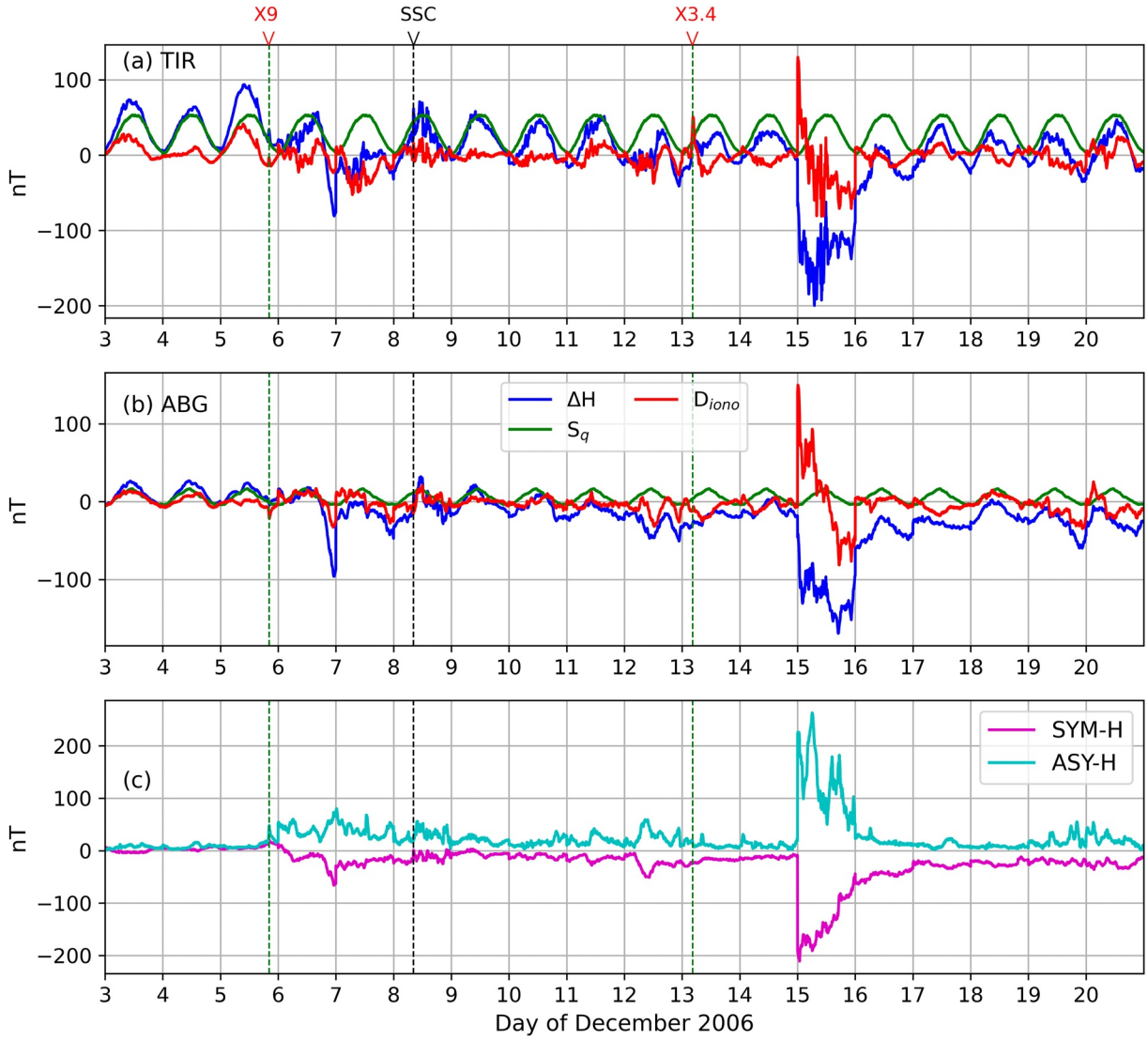

Figure 10. From 3 to 20 December 2006, panel (a) Variations in dayside Earth's magnetic field at TIR (black curves) with the Sq variations (green curve) and D_{iono} (blue curves), panel (b) same curves for ABG, panel (c) SYM-H and ASY-H indices.

(1) The penetration of the magnetospheric convection electric field transmitted from the auroral zone, PPEF (Vasyliunas, 1970)

(2) The disturbed ionospheric dynamo (Blanc & Richmond, 1980) generated by the dissipation of Joule energy from auroral electrojets, DDEF.

These two physical processes affect the magnetic field at low latitudes and generate magnetic field disturbances DP2 for PPEF (Nishida, 1968) and Ddyn for DDEF (Le Huy & Amory-Mazaudier, 2005).

In this section we will separate the two disturbances DP2 and Ddyn using wavelet and semblance techniques.

Figures 10a and 10b show the local variations in dayside horizontal component of Earth's magnetic field (ΔH, blue) along with the quiet time (S_q, green), and ionospheric disturbances (D_{iono}, red) over Indian longitude regions (Tirunelveli (TIR), and Alibag (ABG)) from 3 to 20 December 2006. Some of the flares and SSC (according to Tables 2 and 3 of flares and SSC) are visible at these stations. Figure 10 panel (c) shows the temporal variations in SYM-H, and ASY-H indices corresponding to the same UT. During the geomagnetic storms (SYM-H/ASY-H variations), almost similar patterns in the ΔH component of the geomagnetic field (black line) are seen at both the stations at the same UT. A substantial fall in ΔH can be seen due to enhanced westward ring current during the main phases of both the CIR and CME induced geomagnetic storms on 6th and 15th of December, respectively.

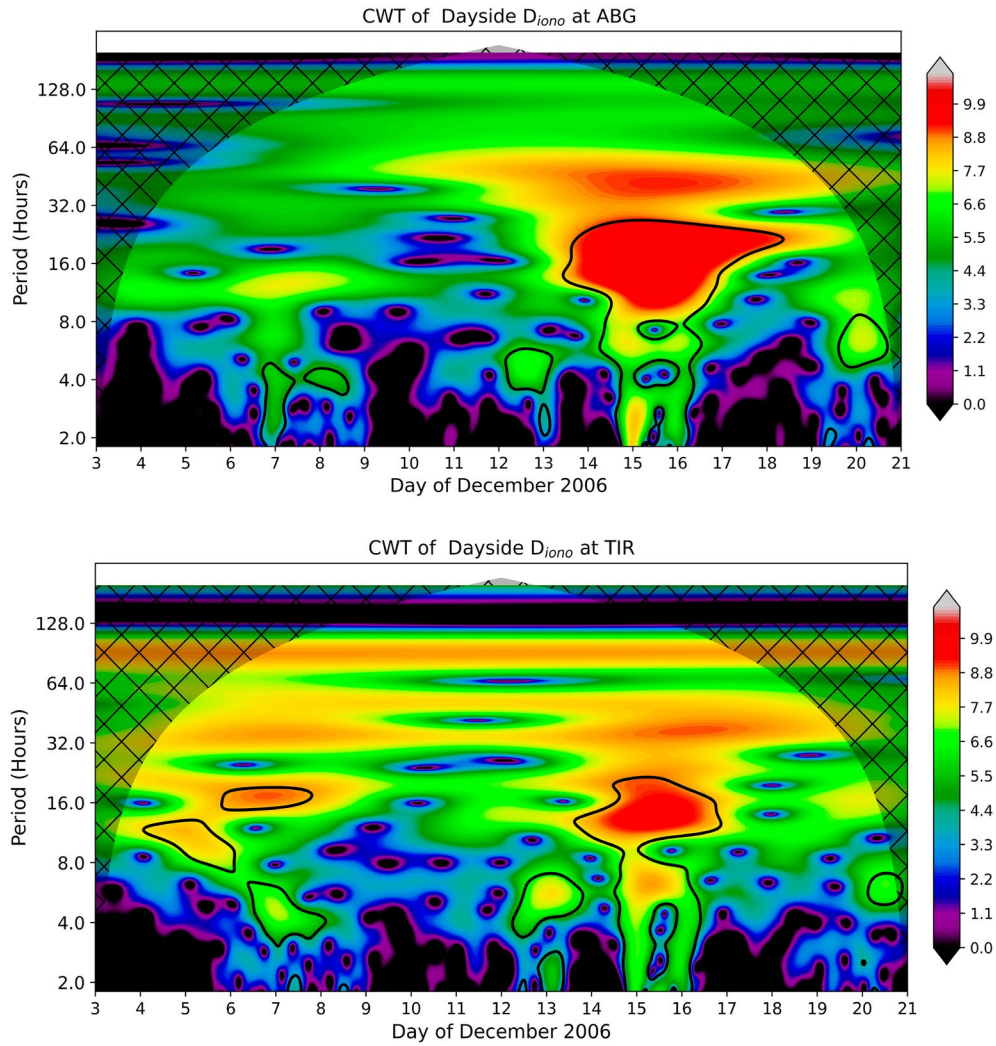

Figure 11. Wavelet analysis of dayside D_{iono} at ABG (top panel) and TIR (bottom panel), from 3 to 20 December 2006.

However, it can also be seen in the figure that a small difference in latitude, and local time for both the stations can still play a crucial role in determining the magnitude of ΔH decrement. The magnitude difference of ΔH variations is also present in D_{iono}(red) variations (Equations 1 and 2), where its pattern seems to be the same at both the stations with difference in magnitude. As the storm starts to recover due to continuously reducing ring current effects (both SYM-H, and ASY-H starts coming back to its controlled values), ΔH variations also start coming back to their pre-storm values.

D_{iono} is the magnetic signature of disturbed ionospheric electric currents circulating on the dayside. At low latitudes D_{iono} is the sum of two magnetic disturbances DP_2 and D_{dyn} (Equations 1–3 in Section 2). The magnetic perturbation DP_2 is composed of short fluctuations (1–3 hr). The signature of the magnetic perturbation D_{dyn} is clearly identified as an anti-Sq circulation on the dayside. At the TIR station we can clearly see the fluctuations of the DP_2 signal every day as well as the anti-Sq signature of D_{dyn} on December 7, 13, 14, 15, and 19, which is discussed further ahead. These days correspond to the impact of CIRs and CMEs. The ABG Station presents a bit different result concerning the anti-Sq disturbance of D_{dyn} observed on the same days. Figure 11 represents the power spectrum of continuous wavelet transformation for D_{iono} during 3–20 December 2006 at both the stations ABG (top panel), and TIR (bottom panel), respectively. Presence of about 12–16 hr period oscillations can clearly be seen at TIR station on 6th–7th of December with high confidence (black contour lines) during the first CIR induced moderate storm and HILDCAA event associated with it. These waves are also present for 14–17 December during and after the CME induced intense geomagnetic storm at both TIR,

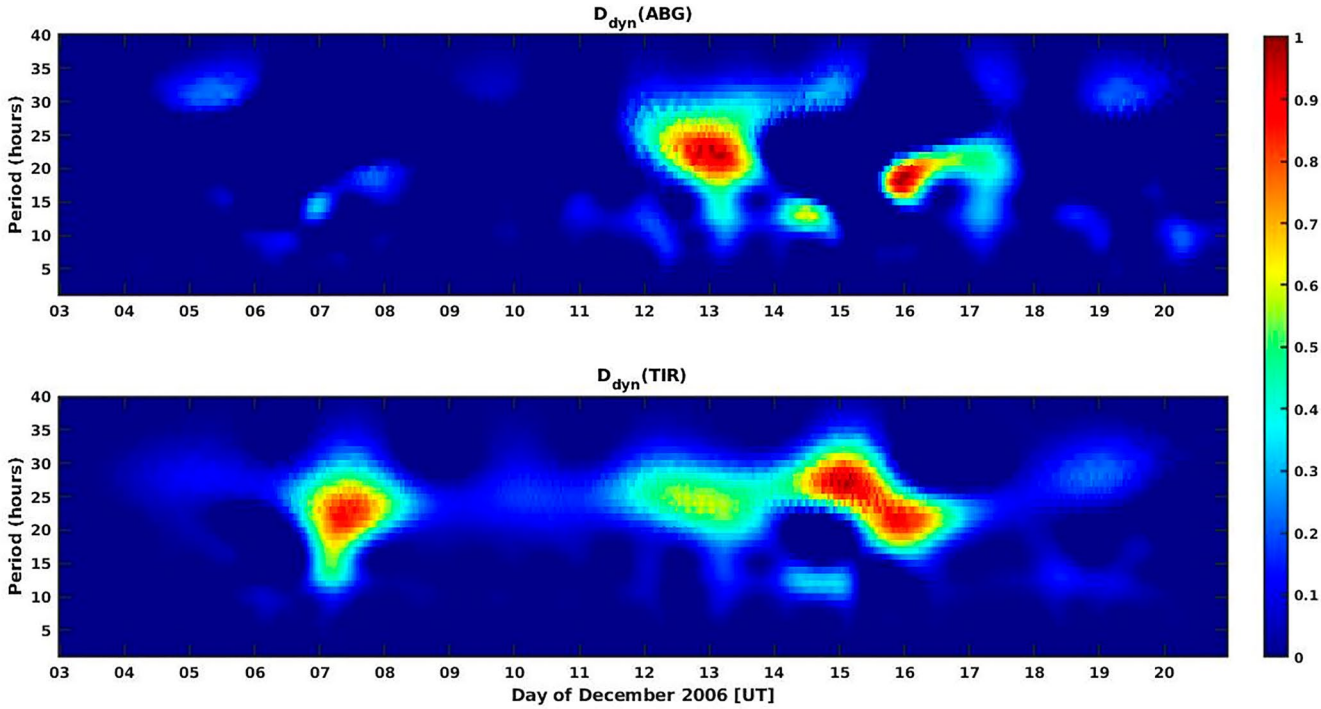

Figure 12. Wavelet + Semblance analysis of D_{dyn} for ABG (top panel) and TIR (bottom panel), from 3 to 20 December 2006.

and ABG. As we are only considering the local dayside for the calculation of D_{iono}, these periodicities could represent the diurnal component associated with the ionospheric DDEF (Blanc & Richmond, 1980; Le Huy & Amory-Mazaudier, 2005; Nava et al., 2016). Short term oscillations of about 1–3 hr due to DP2 fluctuations during PPEF (Nishida, 1968; Vasyliunas, 1970) are also present throughout the storms, which may be associated with continuous IMF-B_z fluctuations during the considered period of our study (Figure 7A, first panel). As can be seen in both the figures, waves of even larger periodicities are also present especially during and after the CME induced storm.

Figure 12 shows the Ddyn disturbance (Equation 3) computed by the wavelet + semblance method (Younas et al., 2022), from 3 to 20 December 2006. The top panel is for the ABG magnetic station and the bottom panel for the TIR one. As theorized by Blanc and Richmond (1980), the ionospheric disturbance dynamo (DDEF) causes a decrease in the day-time Sq currents near the equator. Therefore, an anti-Sq variation observed in the D_{iono} can precisely be linked to Ddyn. In Figure 12, we see an increase in the period of 20–28 hr at ABG on 12, 13, and 17 December 2006, during the second CIR and after the CME. On the other hand, at TIR the signature of DDEF is observed on 6–7 and 12–17 December, during the two CIRs and the CME. It is interesting to notice that the computation of D_{dyn} is in good agreement with the observations of D_{iono} (Figure 10). Indeed, we observe in Figure 10 an anti-Sq variation simultaneous to the D_{dyn} for the station of TIR. For the station ABG there is no anti-Sq circulation for the first CIR (December 6–7) and no D_{dyn}.

D_{dyn} disturbance predicted by Blanc and Richmond (1980) varies with latitude. This disturbance is composed of two equivalent current cells (see Figure 4 of Blanc & Richmond, 1980). The fact that we do not observe equivalent disturbances at ABG and TIR means that these two stations are not on the same portion of the equivalent current cell.

5. Discussion

In this work we analyzed the impact of various solar events (Sfe, CME, CIR, HILDCAA etc.) on the ionosphere over Indian longitudes from December 3 to 20, 2006. Earlier studies have reported few of these variations separately, but no detailed study has been done on the ionosphere over Indian longitudes. We studied the day-to-day variability of ionospheric and magnetic parameters due to succession of the solar disturbances in the light of new scientific findings.

We studied the appearances of crochets in the horizontal component of the Earth's magnetic field observed in the dayside magnetometers at about 10:35 UT on 5th of December due to the intense X-class (X9) solar flare. The impact of this solar flare is also observed in SYM-H and ASY-H indices (Figure 5). The impact in terms of magnitude of enhancement is larger on ASY-H index, compared to SYM-H index. Recently, Liu et al. (2021), using numerical simulations demonstrated "*that solar flare effects extend throughout the geospace via electrodynamic coupling, and are not limited— as previously believed— to the atmospheric region where radiation energy is absorbed*."

The SYM-H and ASY-H indices allow us to know the symmetrical and asymmetrical components of the magnetospheric ring current. The solar flare signatures on SYM-H and ASY-H show that the solar flare impacts on the magnetosphere, this is in agreement with Liu et al. (2021). It is important to note that the magnetometers located on the night side (Figure 5, right side) do not show any impact from the X-class (X9) Sfe.

Gaya-Piqué et al. (2008) studied the X-class (X9) Sfe. They made the equivalent current system due to this Sfe. The equivalent currents are calculated using a two-dimensional model of the ionospheric electric currents closing on the hemisphere which is not the reality. The numerical simulation is based on a three-dimensional approach with a connection between the atmospheric region (where the radiation energy is absorbed) and the magnetosphere. Previous studies (Anad et al., 2016; Mazaudier & Venkateswaran, 1985; Van Sabben, 1961) have already raised the problem of the impossibility of closing regular ionospheric currents only in the ionosphere of one hemisphere. With the work of Liu et al. (2021), the subject is open.

The impact of the X9 solar flare is also seen in ionosphere as a sudden radio fade-out in ionograms (ROQUETES and TIR), and enhanced vTEC in both low to mid-latitude regions due to enhanced ionization of D and E-ionospheric region. Interestingly, the increase in vTEC is larger in mid-latitude (TLSE, and HRAO) compared to low latitudes (IISC and DGAR) (Figure 6a). This could be due to larger increase in conductivity near local noon (TLSE, and HRAO) by the solar flare in comparison to the local late afternoon (IISC, and DGAR) (Figure 1). As can also be seen in Figure 5, the magnetic crochets near TLSE, and HRAO at CLF and HER, respectively, are also stronger in comparison to TIR, and ABG.

Large-scale traveling ionospheric disturbances (LSTIDs) was also observed just after the CME induced intense storm near early UT hours on 15th of December by TIR ionosonde and GPS TEC data sets (Figures 7B and 8b). The TEC perturbations are smaller at DGAR as compared to other stations, which could be due to smaller background TEC in summer (Southern) hemisphere compared to winter (Northern) hemisphere on the same day. Hayashi et al. (2010) also reported multiple LSTIDs near the same UT hours propagating both southward, and northward. However, as can be seen in Figure 8b, based on GPS TEC observation, it's a bit hard to interpret the direction of the LSTID, as the presence of this TID is occurring in late UT hours at both DGAR (southern) and JMSM (northern) from IISC/HYDE.

After a multi-instruments analysis using both ground (ionosonde) and space-based (CHAMP/COSMIC satellites) observations over TIR (magnetic equator), it is found that, there is a positive ionospheric storm over TIR during 7th of December (Figure 7A). At the same time, enhanced Joule heating due to HILDCAA (Figure 4) in high latitude region, and westward electric currents at the equator (Figure 10) are also present. The TIMED/GUVI observed (at about 10 LT) O/N_2 depletion in mid to low-latitude of summer (southern) hemisphere along with O/N_2 enhancement in equatorial to low-latitude of winter (northern) hemisphere in Indian longitude region (over TIR, magnetic equator) (Figure 9e). Which could be due to the enhanced equatorward wind with background summer to winter wind caused by continuous auroral Joule heating (HSS/CIR + ongoing HILDCAA event) present on 7th of December. The presence of WEJ at the same time (7th of December) can suppress the fountain effect over magnetic equator (TIR), and with the enhanced O/N_2 over TIR, it can result in higher electron density over magnetic equator (TIR) than quiet times. The second CIR induced positive ionospheric storm over TIR is also observed during 12–13 December 2006.

The equatorial to low-latitude ionospheric response to CME induced intense geomagnetic storm in Indian longitude region is also presented by investigating the variation of vTEC (Figure 8), and TIR ionosonde observed h′F2 & foF2 (Figure 7A). It is found that there is a negative ionospheric storm on 15th of December with TID occurrence in electron density profile observed by TIR ionosonde, and in the vTEC profile over DGAR station. Which could be due to the compositional (O/N_2) changes (Figure 9m) caused by the UT time of the beginning of the

storm. This negative ionospheric storm is also followed by a positive one on 16th of December. The response of the low latitudes to the CME are well explained by the numerical simulations of Fuller-Rowell et al. (1994, 1996).

We have analyzed the variations of the H component in two Indian stations TIR and ABG (Figure 10). We observe the signature of two known physical processes:

(1) The DP_2 (Nishida, 1968), magnetic signature of the penetration of the magnetospheric convection electric field PPEF (Vasyliunas, 1970). PPEF is the transmission of the magnetospheric convection electric field from auroral zone to low latitudes.

(2) D_{dyn} (Le Huy & Amory-Mazaudier, 2005), magnetic signature of the Ionospheric disturbance Dynamo DDEF (Blanc & Richmond, 1980). In the auroral zone the Joule heating disturbs the thermospheric circulation of winds and generate storm induced meridional winds from the pole to the equator (Amory-Mazaudier et al., 1985; Mazaudier & Bernard, 1985; Mazaudier & Venkateswaran, 1990). These disturbed winds produce electric fields and electric current by dynamo action.

Using Wavelet and Wavelet analysis + semblance analysis we separate these 2 magnetic disturbances (Figures 11 and 12).

Forty years ago, the Saint-Santin incoherent scatter sounder located at middle latitudes allowed observation of the penetration of the magnetospheric convection electric field PPEF (Mazaudier, 1985), by in situ measurements. PPEF is a phenomenon in universal time whose magnetic signature DP_2 is clearly identifiable. In Figures 10 and 11, this phenomenon causes fluctuations of the magnetic field of small periods (<3hr) simultaneous to ABG and TIR. Many articles (more than a thousand) have been published on PPEF. The DP2 magnetic disturbance (Nishida, 1968) due to PPEF, was found experimentally before the theory made by Vasyliunas (1970).

The existence of the disturbed circulation of thermospheric winds during magnetic storms has also been observed with the incoherent scatter sounder (Mazaudier & Bernard, 1985). The amplitude of the wind disturbances observed was in perfect agreement with the simulation of Blanc and Richmond (1980) magnetic disturbance. The wind disturbance by dynamo effect produced disturbed electric field DDEF. The DDEF disturbance was measured by the Jicamarca incoherent scattering sounder located at the magnetic equator (Fejer et al., 1983). But it was only 25 years later that the D_{dyn} magnetic disturbance associated with this phenomenon was isolated for simple cases (Le Huy & Amory-Mazaudier, 2005). The D_{dyn} magnetic disturbance due to perturbed thermospheric winds is a local weather phenomenon that causes an anti-Sq circulation at equatorial latitudes. The extraction of magnetic disturbance associated with perturbed thermospheric winds has been developed during the last decade and different techniques have been used, moving averages (Fathy et al., 2014), Wavelet analysis (Nava et al., 2016), and Wavelet + semblance analysis (Younas et al., 2022). All these studies have highlighted the anti-Sq circulation at low latitudes. However, Blanc and Richmond's model predicts the DDEF disturbance and its associated magnetic signature at the different latitudes of a hemisphere and this is not always anti Sq (see Figure 4 of Blanc and Richmond (1980)). The difference observed between the perturbation D_{dyn} at ABG and TIR (Figure 12) can be explained by Blanc and Richmond's model.

6. Conclusions

In this study we have presented a detailed multi-instrument study of the ionospheric and magnetic variations over India during 3–20 December 2006. This period included an intense solar X9 flare, strongest CME after Halloween storm, HSS with CIR. Many studies have reported the effects of the individual events on the Earth's ionosphere. Our study brings a new understanding of day -to -day variability of the Indian longitude ionosphere under the influence of these space weather events (Solar Flare, CME, and CIR). The ionospheric impact of CIR occurred during December 2006 was not reported earlier. It is only after the IHY project in the 2010s that the study of CIR induced ionospheric perturbation began. The IHY project has changed the geophysical approach to a heliophysical approach and leads to the analysis of the ionospheric variability as a function of the variability of the Sun. This remains as the main motivation of this study.

The current studies are generally focused on understanding the effects of individual events (Solar Flare CME and CIR) and statistics on all phenomena of the same nature. With space weather, we must follow the impact of all solar events on a daily basis and also aim to develop the prediction of their impact on the ionosphere as meteorology does for the lower atmosphere. This is one of the challenges of Space Weather. In our study we have

also addressed the impact of solar and geomagnetic events on the variations of the Earth's magnetic field directly related to the circulation of ionospheric electric currents. We have mainly highlighted the magnetic disturbance D_{dyn} related to the ionospheric dynamo with the new technique of wavelet + semblance. Recall that this disturbance was extracted from the data in 2005 and again it is during the 2010s that the study of this disturbance has developed.

Solar flare induced enhanced conductivity in D and E region ionosphere resulted in small but sudden increase in dayside vTEC, appearance of magnetic crochets, and a total radio blackout at the time of the flare (10:35–10:40 UT, 5 December). Presence of reversed *or* weakened EEJ due to D_{dyn} over Tirunelveli on 7 and 8 December along with the O/N_2 enhancement at the same time resulted in a positive ionospheric storm over the Indian magnetic equator. Enhanced Joule heating induced dynamics in the thermosphere on 15 December resulted in D_{dyn} over TIR, and depletion in O/N_2 at the same time could have played an important role in the observed negative ionospheric storm over Indian longitude regions.

We have been able to fully explain the day-to-day variation of the ionosphere over India with physical phenomena (PPEF, DDEF, change in composition, TID etc.) observed for a long time. The challenge of Space Weather is to integrate all these phenomena in Heliophysical science and also to define their impacts on our widely used technologies such as GNSS (Global Navigation satellite system).

This study also showed the signature of the X9 solar flare of December 5 on the SYM-H and ASY-H indices. A question arises, is this a real impact as a recent numerical simulation shows or is it related to the calculation of SYM-H and ASY-H indices?

Data Availability Statement

Both ground and space based observational data sets are used in this study. Solar X-rays parameters data sets used in this study are available at NOAA National Centers for Environmental Information (2015), https://www.ngdc.noaa.gov/stp/satellite/goes/dataaccess.html (GOES-11), NOAA National Centers for Environmental Information (2022), https://www.ncei.noaa.gov/data/ (GOES-12), and https://www.ias.u-psud.fr/eit/movies/ (GOES-13 and SOHO/EIT). LASCO C2 observed image is available at https://soho.nascom.nasa.gov/pickoftheweek/old/13dec2006/. Solar wind and geomagnetic parameters data sets are available at OMNIWeb interface (Goddard Space Flight Center, OMNIWeb Plus (2006), https://omniweb.gsfc.nasa.gov/), World Data Center for Geomagnetism, Kyoto (2006), https://wdc.kugi.kyoto-u.ac.jp/, and ISGI (https://isgi.unistra.fr/). The ground-based magnetometer data sets used in this study are available at (INTERMAGNET, https://www.intermagnet.org/) and (IIGM, https://www.iigm.res.in/). Space based observation from TIMED/GUVI (TIMED/GUVI (2006), https://spdf.gsfc.nasa.gov/pub/data/timed/guvi/), COSMIC- 1 (University Corporation for Atmospheric Research (2022), https://data.cosmic.ucar.edu/gnss-ro/cosmic1/), CHAMP (Information System and Data Center, GFZ (2018), https://isdc.gfz-potsdam.de/champ-isdc/access-to-the-champ-data/) are also utilized in this study. CADDIS (NASA Earthdata (2006), https://cddis.nasa.gov/archive/gnss/data/daily/) and UNAVCO (NSF's Geodetic Facility for the Advancement of Geoscience (GAGE) (2006), https://www.unavco.org/data/gps-gnss/gps-gnss.html) daily RINEX files are used to extract vTEC. The Roquetes/Spain ionosonde data sets are available at (https://ulcar.uml.edu/).

Acknowledgments
We sincerely thank NASA/SPDF OMNIWeb database, TIMED/GUVI, World Data Center (WDC) for Geomagnetism, Kyoto-Japan, INTERMAGNET database, and IGSI database for their openly available data sets used in this study. We also thank technical team of IIG for operating/maintaining the Ionosonde and magnetometer network. We are grateful for the SOHO/EIT, SOHO/LASCO, GOES-11/GOES-12/GOES-13/SXI, COSMIC-1, and CHAMP observed data sets utilized in this study. We also acknowledge the use of CDDIS/UNAVCO provided data sets used in this study. One of the author AKR thanks Ministry of Education, New Delhi for the financial support in the form of graduate assistantship.

References

Afraimovich, E. L., Demyanov, V. V., & Smolkov, G. Y. (2009). The total failures of GPS functioning caused by the powerful solar radio burst on December 13, 2006. *Earth Planets and Space*, *61*(5), 637–641. https://doi.org/10.1186/BF03352940

Amory-Mazaudier, C., Bernard, R., & Venkateswaran, S. V. (1985). Correction to "Saint-Santin Radar observations of lower thermospheric storms". *Journal of Geophysical Research*, *90*(A7), 6685–6686. https://doi.org/10.1029/JA090iA07p06685

Anad, F., Amory-Mazaudier, C., Hamoudi, M., Bourouis, S., Abtout, A., & Yizengaw, E. (2016). Sq solar variation at Medea Observatory (Algeria), from 2008 to 2011. *Advances in Space Research*, *58*(9), 1682–1695. https://doi.org/10.1016/j.asr.2016.06.029

Azzouzi, I., Migoya-Orue, Y., Mazaudier, C. A., Fleury, R., Radicella, S. M., & Touzani, A. (2015). Signatures of solar event at middle and low latitudes in the Europe-African sector, during geomagnetic storms. *Advances in Space Research*, *56*(9), 2040–2055. https://doi.org/10.1016/j.asr.2015.06.010

Blanc, M., & Richmond, A. D. (1980). The ionospheric disturbance dynamo. *Journal of Geophysical Research*, *85*(A4), 1669–1686. https://doi.org/10.1029/JA085iA04p01669

Carrano, C. S., Bridgwood, C. T., & Groves, K. M. (2009). Impacts of the December 2006 solar radio bursts on the performance of GPS. *Radio Science*, *44*(01), 1–12. https://doi.org/10.1029/2008RS004071

Cerruti, A. P., Kintner, P. M., Jr., Gary, D. E., Mannucci, A. J., Meyer, R. F., Doherty, P., & Coster, A. J. (2008). Effect of intense December 2006 solar radio bursts on GPS receivers. *Space Weather*, *6*(10). https://doi.org/10.1029/2007SW000375

Chakraborty, S., Ruohoniemi, J. M., Baker, J. B. H., & Nishitani, N. (2018). Characterization of short-wave fadeout seen in daytime SuperDARN ground scatter observations. *Radio Science*, *53*(4), 472–484. https://doi.org/10.1002/2017RS006488

Chen, Y., Liu, L., Le, H., & Zhang, H. (2021). Latitudinal dependence of daytime electron density bite-out in the ionospheric F2-layer. *Journal of Geophysical Research: Space Physics*, *126*(1), e2020JA028277. https://doi.org/10.1029/2020JA028277

Curto, J. J. (2020). Geomagnetic solar flare effects: A review. *Journal of Space Weather and Space Climate*, *10*, 27. https://doi.org/10.1051/swsc/2020027

Curto, J. J., Amory-Mazaudier, C., Torta, J. M., & Menvielle, M. (1994). Solar flare effects at Ebre: Regular and reversed solar flare effects, statistical analysis (1953 to 1985), a global case study and a model of elliptical ionospheric currents. *Journal of Geophysical Research*, *99*(A3), 3945–3954. https://doi.org/10.1029/93JA02270

Fathy, I., Amory-Mazaudier, C., Fathy, A., Mahrous, A. M., Yumoto, K., & Ghamry, E. (2014). Ionospheric disturbance dynamo associated to a coronal hole: Case study of 5–10 April 2010. *Journal of Geophysical Research: Space Physics*, *119*(5), 4120–4133. https://doi.org/10.1002/2013JA019510

Fejer, B. G., Larsen, M. F., & Farley, D. T. (1983). Equatorial disturbance dynamo electric field. *Geophysical Research Letter*, *10*(7), 537–540. https://doi.org/10.1029/GL010i007p00537

Fujiwara, H., Maeda, S., Fukunishi, H., Fuller-Rowell, T. J., & Evans, D. S. (1996). Global variations of thermospheric winds and temperatures caused by substorm energy injection. *Journal of Geophysical Research*, *101*(A1), 225–239. https://doi.org/10.1029/95JA01157

Fukushima, N., & Kamide, Y. (1973). Partial ring current models for worldwide geomagnetic disturbances. *Reviews of Geophysics*, *11*(4), 795–853. https://doi.org/10.1029/RG011i004p00795

Fuller-Rowell, T. J., Codrescu, M. V., Moffett, R. J., & Quegan, S. (1994). Response of the thermosphere and ionosphere to geomagnetic storms. *Journal of Geophysical Research*, *99*(A3), 3893–3914. https://doi.org/10.1029/93JA02015

Fuller-Rowell, T. J., Codrescu, M. V., Rishbeth, H., Moffett, R. J., & Quegan, S. (1996). On the seasonal response of the thermosphere and ionosphere to geomagnetic storms. *Journal of Geophysical Research*, *101*(A2), 2343–2353. https://doi.org/10.1029/95JA01614

Futaana, Y., Barabash, S., Yamauchi, M., McKenna-Lawlor, S., Lundin, R., Luhmann, J. G., et al. (2008). Mars Express and Venus Express multi-point observations of geoeffective solar flare events in December 2006. *Planetary and Space Science*, *56*(6), 873–880. https://doi.org/10.1016/j.pss.2007.10.014

Gaya-Piqué, L. R., Curto, J. J., Torta, J. M., & Chulliat, A. (2008). Equivalent ionospheric currents for the 5 December 2006 solar flare effect determined from spherical cap harmonic analysis. *Journal of Geophysical Research*, *113*(A7), A07304. https://doi.org/10.1029/2007JA012934

Goddard Space Flight Center, OMNIWeb Plus. (2006). Solar wind parameters and space weather indices [Dataset]. Retrieved from https://omniweb.gsfc.nasa.gov/

Gopalswamy, N. (2022). The Sun and space weather. *Atmosphere*, *13*(11), 1781. https://doi.org/10.3390/atmos13111781

Hayashi, H., Nishitani, N., Ogawa, T., Otsuka, Y., Tsugawa, T., Hosokawa, K., & Saito, A. (2010). Large-scale traveling ionospheric disturbance observed by superDARN Hokkaido HF radar and GPS networks on 15 December 2006. *Journal of Geophysical Research*, *115*(A6), A06309. https://doi.org/10.1029/2009JA014297

Hofmann-Wellenhof, B., Lichtenegger, H., & Collins, J. (1992). *Global positioning system: Theory and practice*. Springer-Verlag.

Hofmann-Wellenhof, B., Lichtenegger, H., & Collins, J. (2001). *Global positioning system, theory and practice* (5th edition). Springer-Verlag Wien GmbH. https://doi.org/10.10007/978-3-7091-6199-9

Information System and Data Center, GFZ. (2018). CHAMP electron density [Dataset]. Retrieved from https://isdc.gfz-potsdam.de/champ-isdc/access-to-the-champ-data/

International Real-time Magnetic Observatory Network. (2006). The ground-based magnetometer datasets [Dataset]. Retrieved from https://www.intermagnet.org/

International Service of Geomagnetic Indices. (2006). Ap, and Kp geomagnetic indices [Dataset]. Retrieved from https://isgi.unistra.fr/

Kane, R. P. (2006). Are the double-peaks in solar indices during solar maxima of cycle 23 reflected in ionospheric foF2? *Journal of Atmospheric and Solar-Terrestrial Physics*, *68*(8), 877–880. https://doi.org/10.1016/j.jastp.2006.02.003

Kataoka, R., Ebisuzaki, T., Kusano, K., Shiota, D., Inoue, S., Yamamoto, T. T., & Tokumaru, M. (2009). Three-dimensional MHD modeling of the solar wind structures associated with 13 December 2006 coronal mass ejection. *Journal of Geophysical Research*, *114*(A10), A10102. https://doi.org/10.1029/2009JA014167

Le, G., Russell, C. T., & Takahashi, K. (2004). Morphology of the ring current derived from magnetic field observations. In *Annales geophysicae* (Vol. 22, pp. 1267–1295). Copernicus Publications. https://doi.org/10.5194/angeo-22-1267-2004

Le Huy, M., & Amory-Mazaudier, C. (2005). Magnetic signature of the ionospheric disturbance dynamo at equatorial latitudes:"D_{dyn}". *Journal of Geophysical Research*, *110*(A10), A10301. https://doi.org/10.1029/2004JA010578

Lei, J., Wang, W., Burns, A. G., Solomon, S. C., Richmond, A. D., Wiltberger, M., et al. (2008). Observations and simulations of the ionospheric and thermospheric response to the December 2006 geomagnetic storm: Initial phase. *Journal of Geophysical Research*, *113*(A1), A01314. https://doi.org/10.1029/2007JA012807

Lemaire, J. F., & Gringauz, K. I. (1998). *The Earth's plasmasphere*. Cambridge University Press.

J. Lilensten (Ed.) (2007). *Space weather: Research towards applications in Europe* (Vol. 344). Springer Science & Business Media.

Liu, J., Qian, L., Maute, A., Wang, W., Richmond, A. D., Chen, J., et al. (2021). Electrodynamical coupling of the geospace system during solar flares. *Journal of Geophysical Research: Space Physics*, *126*(1), e2020JA028569. https://doi.org/10.1029/2020JA028569

Liu, Y., Luhmann, J. G., Müller-Mellin, R., Schroeder, P. C., Wang, L., Lin, R. P., et al. (2008). A comprehensive view of the 2006 December 13 CME: From the Sun to interplanetary space. *The Astrophysical Journal*, *689*(1), 563–571. https://doi.org/10.1086/592031

Mazaudier, C. (1985). Electric currents above Saint-Santin: 3- A preliminary study of disturbances: June 6, 1978; March 22, 1979; March 23, 1979. *Journal of Geophysical Research*, *90*(A2), 1355–1366. https://doi.org/10.1029/JA090iA02p01355

Mazaudier, C., & Bernard, R. (1985). Saint-Santin radar observations of lower thermospheric storms. *Journal of Geophysical Research*, *90*(A3), 2885–2895. https://doi.org/10.1029/JA090iA03p02885

Mazaudier, C., & Venkateswaran, S. V. (1985). Strange currents over Saint-Santin. *Journal of Geophysical Research*, *90*(A10), 9727–9735. https://doi.org/10.1029/JA090iA10p09727

Mazaudier, C., & Venkateswaran, S. V. (1990). Delayed ionospheric effects of the geomagnetic storms of March 22, 1979 studied by the sixth co-ordinated data analysis workshop (CDAW-6). In *Annales geophysicae* (Vol. 8, pp. 511–518).

Mendillo, M. (2006). Storms in the ionosphere: Patterns and processes for total electron content. *Reviews of Geophysics*, *44*(4). https://doi.org/10.1029/2005RG000193

NASA Earthdata. (2006). CDDIS RINEX files to extract vTEC [Dataset]. Retrieved from https://cddis.nasa.gov/archive/gnss/data/daily

Nava, B., Rodríguez-Zuluaga, J., Alazo-Cuartas, K., Kashcheyev, A., Migoya-Orué, Y., Radicella, S. M., et al. (2016). Middle- and low-latitude ionosphere response to 2015 St. Patrick's Day geomagnetic storm. *Journal of Geophysical Research: Space Physics*, *121*(4), 3421–3438. https://doi.org/10.1002/2015JA022299

Nishida, A. (1968). Geomagnetic D_p 2 fluctuations and associated magnetospheric phenomena. *Journal of Geophysical Research*, *73*(5), 1795–1803. https://doi.org/10.1029/JA073i005p01795

NOAA National Centers for Environmental Information. (2015). GOES-11 data product [Dataset]. Retrieved from https://www.ngdc.noaa.gov/stp/satellite/goes/dataaccess.html

NOAA National Centers for Environmental Information. (2022). GOES-12 X-ray image data product [Dataset]. Retrieved from https://www.ncei.noaa.gov/data/

NSF's Geodetic Facility for the Advancement of Geoscience (GAGE). (2006). UNAVCO RINEX files to extract vTEC [Dataset]. Retrieved from https://www.unavco.org/data/gps-gnss/gps-gnss.html

Pedatella, N. M., Lei, J., Larson, K. M., & Forbes, J. M. (2009). Observations of the ionospheric response to the 15 December 2006 geomagnetic storm: Long-duration positive storm effect. *Journal of Geophysical Research*, *114*(A12), A12313. https://doi.org/10.1029/2009JA014568

Prölss, G. W. (1993). Common origin of positive ionospheric storms at middle latitudes and the geomagnetic activity effect at low latitudes. *Journal of Geophysical Research*, *98*(A4), 5981–5991. https://doi.org/10.1029/92JA02777

Rastogi, R. G., Pathan, B. M., Rao, D. R. K., Sastry, T. S., & Sastry, J. H. (1999). Solar flare effects on the geomagnetic elements during normal and counter electrojet periods. *Earth Planets and Space*, *51*(9), 947–957. https://doi.org/10.1186/BF03351565

Rishbeth, H. (1998). How the thermospheric circulation affects the ionospheric F2-layer. *Journal of Atmospheric and Solar-Terrestrial Physics*, *60*(14), 1385–1402. https://doi.org/10.1016/S1364-6826(98)00062-5

Rother, M., & Michaelis, I. (2019). *CH-ME-2-PLPT—CHAMP electron density and temperature time series in low time resolution (level 2)*. GFZ Data Services. https://doi.org/10.5880/GFZ.2.3.2019.007

Rout, D., Pandey, K., Chakrabarty, D., Sekar, R., & Lu, X. (2019). Significant electric field perturbations in low latitude ionosphere due to the passage of two consecutive ICMEs during 6–8 September 2017. *Journal of Geophysical Research: Space Physics*, *124*(11), 9494–9510. https://doi.org/10.1029/2019JA027133

Schaer, S. (1999). Mapping and predicting the Earth's ionosphere using the global positioning system. Ph.D. thesis. (p. 228). Bern University.

Sripathi, S., Balachandran, N., Veenadhari, B., Singh, R., & Emperumal, K. (2013). Response of the equatorial and low-latitude ionosphere to an intense X-class solar flare (X7/2B) as observed on 09 August 2011. *Journal of Geophysical Research: Space Physics*, *118*(5), 2648–2659. https://doi.org/10.1002/jgra.50267

Sripathi, S., Sripathi, S., Sreekumar, S., Banola, S., Emperumal, K., Tiwari, P., & Kumar, B. S. (2015). Low-latitude ionosphere response to super geomagnetic storm of 17/18 March 2015: Results from a chain of ground-based observations over Indian sector. *Journal of Geophysical Research: Space Physics*, *120*(12), 10–864. https://doi.org/10.1002/2015JA021509

Strickland, D. J., Meier, R. R., Walterscheid, R. L., Craven, J. D., Christensen, A. B., Paxton, L. J., et al. (2004). Quiet-time seasonal behavior of the thermosphere seen in the far ultraviolet dayglow. *Journal of Geophysical Research*, *109*(A1), A01302. https://doi.org/10.1029/2003JA010220

Tao, C., Nishioka, M., Saito, S., Shiota, D., Watanabe, K., Nishizuka, N., et al. (2020). Statistical analysis of short-wave fadeout for extreme space weather event estimation. *Earth Planets and Space*, *72*(1), 1–16. https://doi.org/10.1186/s40623-020-01278-z

TIMED/GUVI. (2006). O/N_2 ratio data products [Dataset]. Retrieved from https://spdf.gsfc.nasa.gov/pub/data/timed/guvi/

Tsurutani, B. T., Gonzaler, W. D., Gonzaler, A. L. C., Guarnieri, F. L., Gopalswamy, N., Grande, M., et al. (2006). Corotating solar wind streams and recurrent geomagnetic activity: A review. *Journal of Geophysical Research*, *111*(A7), A07S01. https://doi.org/10.1029/2005JA011273

Tsurutani, B. T., Judge, D. L., Guarnieri, F. L., Gangopadhyay, P., Jones, A. R., Nuttall, J., et al. (2005). The October 28, 2003 extreme EUV solar flare and resultant extreme ionospheric effects: Comparison to other Halloween events and the Bastille Day event. *Geophysical Research Letters*, *32*(3), L03S09. https://doi.org/10.1029/2004GL021475

Tsurutani, B. T., Verkhoglyadova, O. P., Mannucci, A. J., Lakhina, G. S., Li, G., & Zank, G. P. (2009). A brief review of "solar flare effects" on the ionosphere. *Radio Science*, *44*(01), 1–14. https://doi.org/10.1029/2008RS004029

University Corporation for Atmospheric Research. (2022). COSMIC-1 electron density profiles. [Dataset]. Retrieved from https://data.cosmic.ucar.edu/gnss-ro/cosmic1/

Van Sabben, D. (1961). Ionospheric current systems of ten IGY-solar flare effects. *Journal of Atmospheric and Terrestrial Physics*, *22*(1), 32–42. https://doi.org/10.1016/0021-9169(61)90175-1

Vasyliunas, V. M. (1970). Mathematical models of magnetospheric convection and its coupling to the ionosphere. In M. McCormac (Ed.), *Particles and fields in the magnetosphere* (pp. 60–71). Springer.

World Data Center for Geomagnetism, Kyoto. (2006). Geomagnetic indices, and IQDs [Dataset]. Retrieved from https://wdc.kugi.kyoto-u.ac.jp/

Younas, W., Khan, M., Amory-Mazaudier, C., & Amaechi, P. O. (2022). Ionospheric response to the coronal hole activity of August 2020: A global multi-instrumental overview. *Space Weather*, *20*(12), e2022SW003176. https://doi.org/10.1029/2022SW003176

Zhang, Y., Paxton, L. J., Morrison, D., Wolven, B., Kil, H., Meng, C.-I., et al. (2004). O/N_2 changes during 1–4 October 2002 storms: IMAGE SI-13 and TIMED/GUVI observations. *Journal of Geophysical Research*, *109*(A10), A10308. https://doi.org/10.1029/2004JA010441